# Flux pinning by $Y_2BaCuO_5$ precipitates and field- and temperature-driven pinning centers in melt-powder-melt-growth processed $YBa_2Cu_3O_7$

P. J. Kung, M. P. Maley, M. E. McHenry,* and J. O. Willis
*Superconductivity Technology Center, MS K763, Los Alamos National Laboratory, Los Alamos, New Mexico 87545*

M. Murakami and S. Tanaka
*Superconductivity Research Laboratory, International Superconductivity Technology Center, 1-10-13 Shinonome, Koto-Ku, Tokyo 135, Japan*

(Received 8 June 1993)

Magnetic hysteresis, flux pinning, and flux creep in melt-powder-melt-growth processed $YBa_2Cu_3O_7$ (Y 1:2:3) containing nominal 0, 25, and 40 mol % concentration of $Y_2BaCuO_5$ (Y 2:1:1) inclusions were investigated. The strong pinning due to 2:1:1-phase precipitates in these samples allows for characterization of the hysteretic response as a function of pinning-site concentration over a large portion of magnetic-field–temperature space. We have found the following: (i) The curves of effective pinning energy $U_{\rm eff}$ versus current density $J$ reveal a diverging behavior of $U_{\rm eff}(J)$ in the low-$J$ regime. This supports the existence of a vortex-glass state, and is a signature of a vanishing resistance as the current density approaches zero. (ii) Both the $U_{\rm eff}$ and the $J$ values obtained from magnetic hysteresis loops were observed to increase with Y 2:1:1 concentration. The appearance of the butterfly-shaped (or "fishtail") hysteresis loops indicates a $J_c$ that is an increasing function of $H$ (or $B$). Moreover, it has been demonstrated that the additional pinning leads to an increase in $U_{\rm eff}$ in an $H$-$T$ region in which the butterfly is developed. The derived effective pinning energy is fit, from the instantaneous experimental relaxation data, to the relation, $U_{\rm eff}(J,T,H)=U_i[G(T)/H^n](J_i/J)^{\mu}$, where $U_i$ is the scale of the activation energy, $G(T)=[1-(T/T_x)^2]^m$, and $T_x$ is close in value to $T_{\rm irr}(H)$ (the irreversibility line of the material). This description breaks down in the vicinity of the "butterfly" peak. We observed two power-law regimes of $J$ dependence of $U_{\rm eff}$ which have $\mu$ values that agree qualitatively with the theoretical predictions ($=\frac{7}{9}$ and $\frac{3}{2}$) for a three-dimensional flux-line lattice.

## I. INTRODUCTION

Weak links and flux pinning are two issues receiving much attention from the scientific community studying high-temperature superconductors (HTSC's). Weak links, which generally occur at grain boundaries, have been attributed to grain misorientation[1] and chemical inhomogeneity at the interfaces.[2] Strong-field dependence of the transport critical current density $J_{ct}$ in the low-field regime,[3] and breakdown in the proportionality between the width of the hysteresis loop ($\Delta M \propto J_c$) and the sample dimension[4] experimentally reveal the presence of weak links. If compositional variations at grain boundaries can be minimized, elimination of weak links is often achieved by mechanical texturing (e.g., rolling or pressing), thermal processing (e.g., melt-texturing), or recrystallization techniques (i.e., grain growth along the preferential direction induced by dopants). In contrast to weak links, which are process sensitive, flux pinning is also related to intrinsic properties and is crystal-structure dependent. In three-dimensional (3D) systems with an Abrikosov flux-line lattice (FLL) (e.g., Y-Ba-Cu-O), second-phase precipitates, dislocations, stacking faults, and twins are expected to effectively pin the flux lines. However, for systems that are nearly two-dimensional (2D) and have pancake vortices (e.g., Bi-Sr-Ca-Cu-O), because of very weak interplanar coupling, strong pinning centers must occur in each $CuO_2$ plane to pin pancake vortices when the field is oriented with a component parallel to the $c$ axis. Even when optimal pinning is achieved, the maximum pinning energy for core pinning of a 2D pancake vortex is still much reduced from that available for a well coupled line vortex. When the magnetic field is applied in the $ab$ plane, flux pinning, on the other hand, is controlled by intrinsic pinning mechanisms.[5] It is energetically favorable for flux lines to stay between the $CuO_2$ planes.

In high-temperature superconductors, because of a short coherence length $\xi$ and a high working temperature ($\sim$77 K), weak flux pinning can lead to a severe problem—thermally activated flux motion or flux creep. This magnetic relaxation process generates significant resistance even at $T \ll T_c$ in a modest magnetic field.[6] As a result, energy dissipation is present at finite current densities, which limits the maximum value of the critical current density $J_c$, and hence a variety of applications of HTSC's. Improvement of flux pinning in HTSC's is, therefore, of great technological interest. The smaller maximum pinning energy available in the most anisotropic, 2D-like compounds makes this difficult to achieve.

The melt-powder-melt-growth (MPMG) process[7,8] has been demonstrated to be effective in fabricating bulk $YBa_2Cu_3O_7$ (Y 1:2:3) superconductors with a minimum of weak links. Additionally, by introducing a fine (0.5–1

 

$\mu$m) dispersion of second-phase inclusions of the $Y_2BaCuO_5$ (Y 2:1:1 phase), which act as pinning centers, $J_c$ of bulk $YBa_2Cu_3O_7$ is much enhanced at elevated temperatures and magnetic fields. It is therefore of great interest to examine the effect of this enhanced pinning on thermally activated flux motion as well as to investigate the variation in pinning with concentration of the Y 2:1:1 phase. Moreover, high-quality MPMG-processed $YBa_2Cu_3O_7$ material, without weak links present, carries significant $J_c$ over a wide range of temperature (5–80 K), which facilitates comparison with the predictions of the collective-pinning[9] and vortex-glass models.[10] The field dependence of magnetic relaxation in these samples has also been investigated in this work. These results can be described by a scaling function for the current-dependent pinning energy $U_{\rm eff}(J,T,H)$. Such a scaling function was first proposed by Maley *et al.*[11] and later employed by McHenry *et al.*[12] in studies of a $La_{1.86}Sr_{0.14}CuO_4$ single crystal. Here we further demonstrate how butterfly or fishtail hysteresis loops[13] (which were observed in one of our samples—Y 1.8), presumably due to the effect of localized low-$T_c$ phases on flux pinning, can influence the $U_{\rm eff}(J,T,H)$ curves. As will be seen, this leads to a crossover effect in the $U_{\rm eff}(J,T,H)$ curves. At a given value of the current density, higher effective pinning energies are observed compared with the ones obtained at lower fields and temperatures in the absence of this additional pinning.

## II. RATIONALE FOR THE MELT-POWDER-MELT-GROWTH (MPMG) PROCESS

The MPMG method has been employed successfully to synthesize large grained bulk $YBa_2Cu_3O_7$ which exhibits large $J_c$'s (exceeding $10^4$ A/cm$^2$ at 77 K). The key to attaining such high $J_c$'s is the enhanced flux pinning by the $Y_2BaCuO_5$ inclusions and the effective grain alignment during the melt growth. The general procedure of the MPMG method can be found elsewhere.[7,8] By careful control of the temperature gradient, the principal growth direction parallel to the gradient is along the *ab* plane of $YBa_2Cu_3O_{7+\delta}$, and hence texturing is easily achieved. To interpret the absence of weak links in the MPMG-processed $YBa_2Cu_3O_7$, a growth mechanism similar to a traditional cellular solidification process has been recently suggested:[14]

(i) At the early stage of crystal growth, parallel platelets within domains are separated by gaps due to the anisotropy in the growth rate along the *ab* plane and the *c* axis. These gaps are subsequently filled with material from the liquid phase and are eventually terminated within the individual domains. The as-synthesized crystals are strongly coupled and behave like single crystals in which no weak-link behavior is observed. Current flow along the direction parallel to the *c* axis is consequently through single-crystal-like regions within a domain of the sample.

(ii) The Y 2:1:1 inclusions are believed not only to serve as nucleation sites for Y 1:2:3 phase but also to enhance the growth rate along the *c* axis.[15] It has been observed that finer Y 2:1:1 particles as well as an increase in the particle density lead to a more frequent layer formation.[16] Therefore, the presence of Y 2:1:1 inclusions results in the three-dimensional growth of bulk Y 1:2:3 superconductor.

Anisotropy in the coefficient of thermal expansion in Y-Ba-Cu-O has been widely recognized as contributing to microcracks along the *ab* plane for melt-textured material. These cracks can reduce the effective supercurrent-carrying dimension of the material and manifest themselves in granular behavior. The addition of Y 2:1:1 inclusions was also found to substantially reduce cracking in textured $YBa_2Cu_3O_7$.[17] Furthermore, the difference in mechanical properties between Y 2:1:1 inclusions and the Y 1:2:3 matrix,[18] as well as the interdiffusion resulting in a compositional variation in the vicinity of the Y 2:1:1/Y 1:2:3 interfaces,[19] can affect to some extent the formation and distribution of microstructural defects.

## III. $Y_2BaCuO_5$ INCLUSIONS, MICROSTRUCTURAL DEFECTS, AND FLUX PINNING

In general, twin planes, dislocations, stacking faults, oxygen vacancies, and second-phase precipitates are common microstructural features observed in Y-Ba-Cu-O superconductors. Twin boundaries occur due to a tetragonal to orthorhombic structural phase transformation which occurs during the cooling process after oxygenation.[19–21] Twins form in order to relieve the stress accompanying this transformation. In polycrystalline Y-Ba-Cu-O, the spacing between twin boundaries within a grain is typically about 200 nm.[22] The twin planes, which extend through the thickness of the crystal (i.e., parallel to the *c* axis), are expected to play a role in enhancing the flux-pinning behavior when the applied magnetic field is low and nearly parallel to the twin planes. Although increasing the number of twins boundaries leads to an increase in $J_c$, this effect is not very significant.[23,24] In MPMG-processed Y 1:2:3 samples, in addition to twins, Y 2:1:1 inclusions, stacking faults, and sometimes microcracks have been observed.[25,26] The Y 2:1:1 inclusions are extended defects and can pin flux lines for both $H\|c$ and $H\perp c$. On the other hand, stacking faults and microcracks are typically in the *ab* plane, and they are more effective in pinning the flux lines when $H\perp c$. In this work, for magnetic measurements we align the *c* axis with the magnetic fields so that pinning mainly due to Y 2:1:1 inclusions can be studied. As compared with Y 2:1:1 inclusions, the twin distribution throughout the sample is not so homogeneous.

The interface between the Y 2:1:1 inclusions and the matrix material has been previously suggested to be important in enhancing flux pinning.[27] However, this idea has been questioned by several groups.[28,29] The major controversy is "How can a Y 2:1:1 inclusion of $\sim 1$ $\mu$m average particle size effectively pin a flux bundle when the superconducting coherence length $\xi$ ($\xi_c \sim 3$ Å, $\xi_{ab} \sim 15$ Å) of Y-Ba-Cu-O is many orders of magnitude smaller?" Murakami and co-workers[27,30,31] have answered this question in the following way.

(i) A soft flux-line lattice (due to a small shear modulus $C_{66}$) in Y-Ba-Cu-O allows fluxons to bend in order to find pinning sites which can be viewed as potential-energy

wells for fluxons. For large volume normal-state defects, the free energy of a flux bundle does not vary with position within the defect. Therefore, fluxons are mainly pinned at the interface between the defect and the superconducting matrix where the gradient in free energy is a maximum. This implies that large defects can pin several flux lines simultaneously at the defect-superconductor interface.

(ii) From the viewpoint of pinning efficiency, if interfacial pinning is operative, a high total interfacial area is important. Thus, small defects are better than large ones.

Although the arguments stated above may not be completely convincing, higher critical current density is experimentally confirmed with increasing Y 2:1:1 concentration in this work. Whether the actual mechanism for enhanced pinning is directly or indirectly caused by the Y 2:1:1 inclusions still requires more investigation. Nevertheless, the functions of Y 2:1:1 in the MPMG-processed samples are proposed as follows.

(i) Suppression of microcracking: Internal strain is often developed in the tetragonal-to-orthorhombic transformation caused by oxygen absorption during oxygen annealing. This strain is usually accommodated by the formation of twin planes along the $c$ axis and by the occurrence of cracks perpendicular to the $c$ axis in melt-textured Y-Ba-Cu-O. The addition of Y 2:1:1 inclusions is postulated to create a strain field which disperses stress and reduces stress concentration arising from the phase transformation thus preventing the formation of cracks.[32] As a result, numerous stacking faults are usually found at the Y 2:1:1/Y 1:2:3 interfaces.[33] Because of this stress relief, no distortion was found at the interface between Y 2:1:1 inclusion and Y 1:2:3 matrix by transmission electron microscopy (TEM) and Fourier transforms of crystal lattice images.[25,26] A thin ($\sim$1 nm) amorphous layer has been occasionally found to exist at the interfaces and may aid in relaxing the stress in the Y 1:2:3 matrix.

(ii) Enhancement of flux pinning: Flux pinning can be mainly due to the interaction between normal-state Y 2:1:1 inclusions and vortices. Structural defects around Y 2:1:1 inclusions may also contribute to flux pinning. For instance, stacking faults and their bounding dislocation loops, as well as the compositional disorder around the Y 2:1:1 inclusions, which causes the formation of precipitates, have been recently suggested to act as point pinning centers in the case of $H \| c$.[33] The presence of Y 2:1:1 probably has an influence on the formation of these defects because many of them terminate at the Y 2:1:1/Y 1:2:3 interfaces.[17,32]

From TEM analysis performed on our MPMG-processed samples, fine spherical or ellipsoidal Y 2:1:1 inclusions were found embedded in the Y 1:2:3 matrix. Very dense twins, which terminate at the Y 2:1:1/Y 1:2:3 interfaces, were also typically seen. However, the twin boundaries were often found to be not exactly parallel to the $c$ axis. Such deviation can affect their effectiveness in pinning and hence the angular dependence of $J_c$.[34] Some unidentified precipitates and many dislocations originating from grain boundaries were also observed.

The average Y 2:1:1 particle size is 0.5–1 $\mu$m, and the average spacing between inclusions is of the order of 1 $\mu$m. Because the starting compositions and the processing conditions can affect these dimensions, a future important work is to correlate these factors with the enhanced pinning behavior due to the Y 2:1:1 phase. For instance, it was observed that addition of Pt in the MPMG process significantly refines the Y 2:1:1 inclusions.[35] With smaller Y 2:1:1 inclusions and a different spacing [i.e., consider the ratio of the vortex-lattice parameter $a_0 = 1.075(\Phi_0/B)^{0.5}$ to the spacing between the pinning centers, where $\Phi_0 = 2.07 \times 10^{-15}$ Wb, one flux quantum], the regimes of magnetic field in which enhanced pinning behavior is observed are expected to change. Recently, it has been experimentally shown that smaller sizes and spacings of Y 2:1:1 inclusions are more effective in enhancing $J_c$ than larger ones.[36] This is partly due to increased pinning of smaller Y 2:1:1 particles, but is probably also related to changes in the defect structure.

Previous studies have shown that oxygen vacancies in Y-Ba-Cu-O can result in the so-called "butterfly" or "fishtail" hysteresis loops. The low-$T_c$ regions associated with these defects are, in principle, driven normal by a combined effect due to temperature and magnetic field and then can pin vortices.[13] In general, the superconducting order parameter can be modulated by oxygen deficiencies and other nonsuperconducting defects influencing the pinning observed in the sample. We shall see the influence of large Y 2:1:1 concentrations on flux creep in the $U_{\text{eff}}(J)$ curves described below. Furthermore, the presence of Y 2:1:1 particles may possibly affect oxygenation and the distribution of oxygen deficient regions in the superconductor and hence flux pinning characteristics.

Using a single-vortex pinning model based on the core-condensation energy, Murakami and co-workers[27,30] derived an expression that indicates $J_c$ to be proportional to the volume fraction of Y 2:1:1 inclusions and inversely to the average Y 2:1:1 particle size. It implies that the efficiency of pinning can be increased by decreasing the size of the pinning sites. The expected field and temperature dependence of $J_c$ from this model is given as $J_c \propto B^{-0.5}$ and $J_c \propto [1-(T/T_c)^2]^{1.5}$. As pointed out by Gyorgy *et al.*,[37] the background pinning contributed by small defects may be dominant at low temperatures. They observed $J_c \propto [1-(T/T_c)^2]^4$. However, according to the collective-pinning theory,[38] $J_c$ was suggested to be proportional to $[1-(T/T_c)^2]^{5.5}$. Therefore, among various systems the actual observed values of the exponents are likely determined by the microstructural details of the samples. In addition, the nature of the flux-line lattice (FLL) is another factor to be considered. The rigidity of the flux-line lattice, which is related to its elastic constants ($C_{11}$, $C_{44}$, and $C_{66}$), can reduce the pinning effectiveness of some pinning centers. The flux bundle volume is proportional to the correlation lengths in the longitudinal and transverse directions.[9] These two correlation lengths are determined by $C_{44}$ and $C_{66}$, the bending and shear moduli, respectively. Therefore, a soft FLL favors collective pinning and requires a statistical summation of the pinning forces over individual pinning sites.[38] The effect of the Y 2:1:1 inclusions on flux pin-

ning obviously can be difficult to distinguish between direct and indirect contributions.

## IV. EXPERIMENTAL DETAILS

Three thin specimens ($\sim$1 mm thick) with orthorhombic shape were cut for magnetic measurements from as-processed $YBa_2Cu_3O_7$ with 0, 25, and 40 mol% of $Y_2BaCuO_5$ inclusions, respectively. The corresponding sample names are Y 1.0, Y 1.5, and Y 1.8. The specimens consisted of several crystals having the same orientation, with the largest surface approximately perpendicular to the $c$ axis. Superconducting transition temperatures ($M$ versus $T$), magnetic irreversibility lines ($T_{irr}$ versus $H_{irr}$), magnetic hysteresis ($M$ versus $H$), and relaxation ($M$ versus $t$) were measured using a superconducting quantum interference device (SQUID) magnetometer (MPMS, Quantum Design). "MARZ" grade palladium samples are employed as the calibration samples to verify the overall calibration of the magnetometer. The measured magnetic moment is calibrated for these palladium samples of mass between 0.225 and 0.275 g. The differential sensitivity of the SQUID is about $10^{-8}$ emu and temperature stability below 100 K is $\pm 0.5\%$. Because field inhomogeneity in the solenoidal magnet of the magnetometer can cause the sample to undergo minor hysteresis loops during travel through the SQUID coils,[39] a scan length of 3 cm is used in order to minimize the inhomogeneity of the magnetic field. This leads to field variation less than 0.05%.

To precisely orient the $c$ axis with the field the specimen was oriented using Laue diffraction and mounted on a Kel-F disk. Misalignment can cause experimental errors in the magnetization data. Rotation of the sample by an induced torque from the applied field may also occur if the sample is not mounted rigidly. To examine intergranular coupling, samples were cut in half along both the $c$ axis and the $ab$ plane directions, and magnetic hysteresis was measured before and after cutting.

For the measurements of magnetic relaxation, the sample was cooled in zero field, the applied magnetic field was raised to 5 T and then lowered to the selected value, and the isothermal magnetization $M$ as a function of time was recorded at every 60, 120, 240 sec for a total time of 3–4 h. The procedure is repeated at various temperatures and fields in order to determine $U_{eff}(J,T,H)$. $M(t)$ behavior in applied magnetic fields of 1, 2, 3, and 4 T in the temperature range of 5–80 K was investigated. In the low-temperature regime, flux jumps causing a change in the magnitude of the magnetic moment may take place; however, no such behavior was observed during any of the measurements discussed here.

## V. PHENOMENOLOGICAL MODELS AND DATA ANALYSIS OF MAGNETIC RELAXATION

At high temperatures, because of higher thermal energy and lower activation energy, the dissipative effect caused by thermally activated motion (or flux creep) aided by the Lorentz force is more severe in HTSC's than in conventional superconductors. To avoid energy dissipation, strong pinning centers must be introduced. Several phenomenological models have been proposed to describe flux creep. The main difference among these models is the expression for the current-dependent effective pinning energy, $U_{eff}(J)$. Nevertheless, an Arrhenius form for the hop rate $\nu$ is a universal feature:

$$\nu=\nu_0 \exp\left[-\frac{U_{eff}(J)}{kT}\right], \tag{1}$$

where $\nu_0$ is an attempt frequency and $U_{eff}(J)$ is the effective activation energy for flux lines jumping over pinning barriers. In the presence of a gradient in the magnetic-flux density or of a transport current in the superconductor, a Lorentz force energy will reduce the pinning energy barrier. When a magnetic field is first applied, the flux profile penetrates the superconductor and magnetic relaxation starts from the critical state where $J \cong J_c$ and $U_{eff}(J_c) \cong 0$. A net thermally activated flux flow is then induced preferentially down the flux gradient. To describe this process, Anderson[40] and Kim, Hempstead, and Strnad[41] assumed a linear $J$-dependent form for the effective activation energy,

$$U_{eff}(J)=U_0-JBVa=U_0\left[1-\frac{J}{J_c}\right], \tag{2}$$

where $J$ is the current density, $B$ is the magnetic induction, $V$ is the flux bundle volume, and $a$ is a hop distance. $U_0$ is a volume average value for the full activation energy (i.e., the average pinning well depth) at zero current density (or $JB \sim 0$). By definition, $J_c$ is the current density for which $U_{eff}(J)$ is zero. However, as first pointed out by Beasley, Labusch, and Webb[42] for realistic forms of the pinning potential, a nonlinear dependence for $U_{eff}(J)$ must be assumed. Instead, starting with the flux conservation equation:

$$\frac{dB}{dt}=\nabla\left[Ba\omega_0 \exp\left[-\frac{U_{eff}(J)}{kT}\right]\right], \tag{3}$$

where $\omega_0$ is a characteristic attempt frequency, and $a$ is a hop distance. For $U_{eff}(J)$, a treatment of flux diffusion can be derived without assuming linearity. For simplicity, here we consider a one-dimensional geometry for a slab of thickness $d$. Equation (3) can be integrated over the slab volume to obtain a partial differential equation for the spatially averaged magnetic induction as determined by diffusion through the sample surface:

$$\frac{d\langle B\rangle}{dt}=4\pi\frac{dM}{dt}=\left[\frac{4Ba\omega_0}{d}\right]\exp\left[-\frac{U_{eff}(J)}{kT}\right]. \tag{4}$$

$U_{eff}(J)$ can be further solved for by algebraic rearrangement of Eq. (4) to yield

$$\begin{aligned}\frac{U_{eff}(J)}{k}&=-T\ln\left|\frac{dM}{dt}\right|+T\ln\left[\frac{Ba\omega_0}{\pi d}\right]\\&=-T\left[\ln\left|\frac{dM}{dt}\right|-C\right],\end{aligned} \tag{5}$$

where $C=\ln(Ba\omega_0/\pi d)$, which can be treated as a con-

stant at low temperatures. In this work, we determine its value by fitting the instantaneous experimental relaxation data, $T\ln|dM/dt|$ versus $M$, to give the smoothest continuous fit of the low-temperature ( $\leq 15$ K) $U_{\rm eff}$ versus $M$ data. As will be seen later, a single value of $C$ for each field does not result in a smooth curve over a wide range of temperature, especially for the high-temperature data. In order to account for the implicit temperature dependence of $U_{\rm eff}$, we then investigate the possible expressions for a temperature scaling function, $G(T)$ that ensures continuity at high temperatures. The typical form is given as[12,43]

$$G(T)=\left[1-\left[\frac{T}{T_x}\right]^2\right]^m, \tag{6}$$

where $1\leq m\leq 2$ and $T_x$ is a characteristic temperature used as a fitting parameter to align the high-temperature data so that a continuous curve of $U_{\rm eff}/kG(T)$ versus $M$ is obtained. $T_x$ roughly approximates the irreversibility temperature $T_{\rm irr}$. An early discussion as to choosing the function $G(T)$ has been given by McHenry *et al.*[12] More recent work suggests that a specific functional expression for $G(T)$ may not be universally correct for obtaining a smooth curve $U_{\rm eff}/kG(T)$ versus $M$.[44] Finding alternate methods for determining this function is one of the objectives of this work.

One alternative for determining $G(T)$, the condition for continuity of $U_{\rm eff}$ is considered. Beginning with the lowest temperature data, each isothermal $M(t)$ set is multiplied by a scaling factor such that it forms a continuous smooth $U_{\rm eff}(J)$ curve with the data sets recorded at the two adjacent lower temperatures.[44] The scaling factor is introduced so as to require continuity of the high-temperature data sets with the smooth curve extrapolated from the low-temperature data. By doing so, the scaling function $G(T)$ is implicitly determined from the scaling factors and subsequently a specific functional form can be determined by curve fitting this $G(T)$ data set.

Magnetic-field scaling of $U_{\rm eff}/kG(T)$ is determined using an $H^n$ power law such that the $U_{\rm eff}(J)/kG(T)$ curves at all fields can be superimposed. The final expression for $U_{\rm eff}(J,T,H)$, which takes into account the nonlinear current dependence of activation energy as well as field and temperature scaling, is thus given empirically as

$$U_{\rm eff}(J,T,H)=U_i\frac{G(T)}{H^n}F\left[\frac{J_i}{J}\right], \tag{7}$$

where $U_i$ and $J_i$ are scaling values that depend upon $J/J_c$.[9]

Finally, to determine the functional form for $F(J_i/J)$, we need to extract $J$ from the magnetization curve. With the aid of the Bean model,[45,46] the magnetization $M$ (emu/cm$^3$) obtained from relaxation measurements can be converted into $J$ (A/cm$^2$) if the scaling length for supercurrent flow in the sample is known and suitable corrections are made for equilibrium and addenda magnetizations. These corrections include the following.

(i) The magnetization of the Kel-F sample holder: This is especially important at high temperatures where the Kel-F contribution to $M$ is comparable to the small $M$ value of the sample. The diamagnetic contribution of the Kel-F is routinely subtracted.

(ii) The reversible magnetization $M_{\rm rev}$: In the calculation of $J_{cm}$ from the width of hysteresis loops, $M_{\rm rev}$'s obtained from the increasing and decreasing branches cancel out. In magnetic relaxation measurements on one branch of the hysteresis curve, $M_{\rm rev}$ must be subtracted from $M$. In this work, $M_{\rm rev}$ was obtained both from averaging field increasing and decreasing branches of the hysteresis loops and from extrapolations of $M_{\rm rev}$ from above the irreversibility line.

By doing so, we obtain the true irreversible component of the magnetization, $M_{\rm irr}$, using the following expression:

$$M_{\rm irr}=M_{\rm measured}-M_{\text{Kel-F}}-M_{\rm rev}\ . \tag{8}$$

The magnetization current density $J_m$ (A/cm$^2$) is then calculated from $M_{\rm irr}$ (emu/cm$^3$) by[47]

$$J_m=\frac{20M_{\rm irr}}{a[1-(a/3b)]} \tag{9}$$

for an orthorhombic cross section ($a$ and $b$ are the width and the length; $b>a$).

After determining the true irreversible component of the magnetization, the current density dependence of $U_{\rm eff}(J)$ and $F(J_i/J)$ can be determined. Both logarithmic and power-law fits have been considered {i.e., $U_{\rm eff}/kG(T)$ versus $\log_{10}J$ or $\log_{10}[U_{\rm eff}/kG(T)]$ versus $\log_{10}J$} here. The logarithmic $U_{\rm eff}(J)$ dependence was previously found to well describe the $I$-$V$ characteristics of transport current flow in $YBa_2Cu_3O_{7-\delta}$ epitaxial films within the framework of the flux-creep model,[48]

$$U_{\rm eff}\left[\frac{T}{T_c},J,H\right]=U_j\left[\frac{T}{T_c},H\right]\ln\left[\frac{J_c}{J}\right], \tag{10}$$

where $U_j$ is the scale of the activation energy, and $J_c$ is the critical current at $U_{\rm eff}\approx 0$. Models based on vortex-glass and collective-pinning–collective flux-creep theories, on the other hand, have derived an inverse power-law expression for $U_{\rm eff}(J)$ that can be generally written as[9,10]

$$U_{\rm eff}(J)\cong U_i\left[\frac{J_i}{J}\right]^{\mu}, \tag{11}$$

where $J_i$ is the current density and the exponent $\mu$ is of order 1 for the vortex-glass model. $J_i$ and $\mu$ both vary with the dimensionality of the vortex lattice and with the value of $J_i/J$ in the collective creep model. Because the collective-pinning–collective flux-creep model considers the current dependence of the flux bundle volume, different regimes of the bundle size lead to different power-law regimes. In the case of three-dimensional (3D) systems of the flux-line lattice, $\mu=\frac{7}{9}$, $\frac{3}{2}$, and $\frac{1}{7}$ correspond to regimes of flux creep caused by large vortex bundles ($\gg\lambda$), small vortex bundles ($\ll\lambda$), and single-vortex lines, respectively. Alternatively, they correspond to different regimes of $J/J_c$, which are accessed at different temperatures in this measurement, with the smaller bundle sizes observable at lower temperatures (higher $J/J_c$).

In order to meet the boundary condition $U_{\rm eff}=0$ at

$J=J_c$ and express it explicitly, Eq. (11) can be modified without changing the physical picture to give the form[49]

$$U_{\text{eff}}(J)=U_i\left[\left[\frac{J_c}{J}\right]^{\mu}-1\right]. \quad (12)$$

Multiple power-law regimes are commonly observed in our MPMG-processed samples and are consistent with the results of vortex-glass and collective flux-creep models for a 3D system.[9,10,50] These power-law expressions can be used to distinguish between different flux-pinning mechanisms and especially the behavior that reflects different dimensionalities of the vortex lattice (two or three dimensional).[51,52]

## VI. RESULTS AND DISCUSSION

### A. Irreversibility line and magnetic hysteresis

All three MPMG-processed samples exhibit sharp diamagnetic transitions at 92 K in a field of 10 Oe, which suggests that the samples consist of a nearly homogeneous $YBa_2Cu_3O_7$ phase. In Fig. 1(a), the Meissner (flux expulsion) fraction of less than 1% observed in these samples implies very strong flux pinning. The irreversibility line, $T_{\text{irr}}(H_{\text{irr}})$, is obtained from the points at which the zero-field-cooled and field-cooled magnetizations first coincide for magnetic fields ranging from 10 Oe to 50 kOe as shown in Fig. 1(b). The data fit the relation, $1-T_{\text{irr}}/T_c \sim H_{\text{irr}}^n$ approximately with $\frac{1}{3}\le n\le\frac{2}{3}$. The field dependence of $T_{\text{irr}}$ decreases slightly with increasing concentration of the Y 2:1:1 phase.

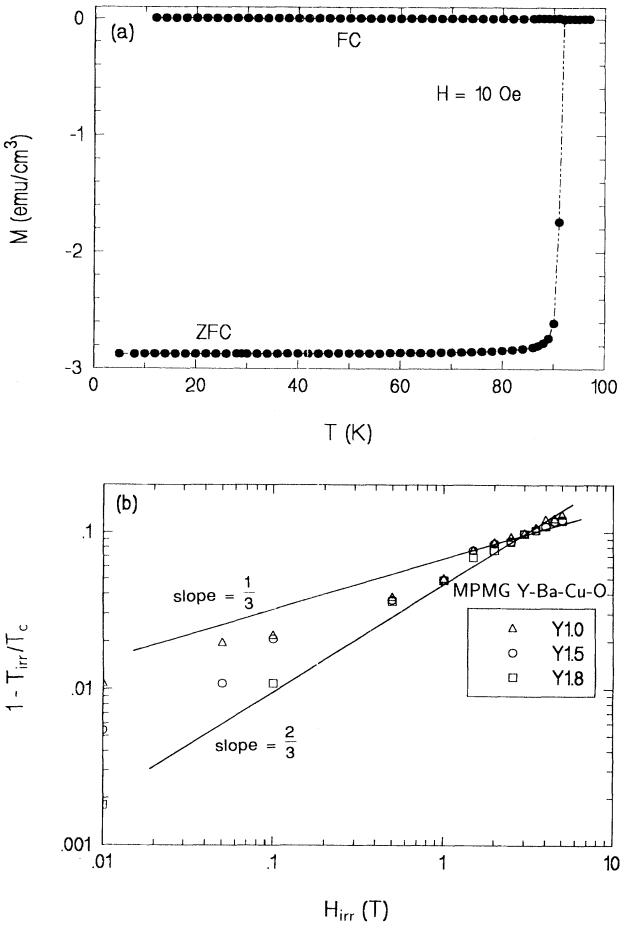


FIG. 1. (a) A typical sharp superconducting transition curve with $T_c=92$ K ($H=10$ Oe) in which the Meissner effect is less than 1%, and (b) magnetic irreversibility lines of the MPMG-processed $YBa_2Cu_3O_7$ samples. Solid lines are a fit to the relation $1-T_{\text{irr}}/T_c \sim H_{\text{irr}}^n$, where $n=\frac{1}{3}$ and $\frac{2}{3}$.

In order to derive the critical current density from the magnetization, the effective dimension for supercurrent flow must be first determined. According to the Bean model,[45,46] $J_c=c(\Delta M/d)$ (where $c$ is a constant, $\Delta M$ is the width of the hysteresis loop, and $d$ is the transverse dimension), is valid only when the entire sample is in the critical state and assumes that $J_c$ is independent of $H$. Thus, identifying the value of $d$ is important. In bulk superconductors, a high applied magnetic field or high temperature can cause a network of percolative weak links (i.e., individual superconducting regions connected by normal or insulating tunnel barriers at grain or subgrain boundaries). Eventually these regions become completely decoupled by field or temperature and hence exhibit low transport critical current density. This observation suggests that a transition from intergranular $J_c$ to intragranular $J_c$ may occur in a polycrystalline sample. If the sample exhibits strong intergranular coupling, $\Delta M$ is proportional to the sample dimension perpendicular to the field which is then used as $d$.[7] On the other hand, for a completely decoupled sample, the grain size is more appropriate for the $d$ value.[53,54] Because magnetic relaxation takes place while the applied magnetic field is ramping, critical current density determined in this way also depends on the sweep rate of the applied field.

Figure 2 illustrates typical features of hysteresis loops for samples measured as a whole (i.e., uncut) and for a cut sample (i.e., approximately one-half the dimension of the original one). The solid line was obtained from data taken for the cut piece by scaling with the change in its dimension in accordance with the Bean model expression. This solid line is identical with the hysteresis loop obtained from the uncut sample except for the regime near zero field, which differs due to demagnetization effects. Obviously, the sample in both orientations (i.e., $H\|c$ and $H\perp c$) gives a linear dependence of $M$ on $d$, implying that the current circulates around the entire sample. The difference in the magnitude of $M$ between these two orientations suggests the anisotropy in their corresponding $J_c$'s.

### B. Field and temperature dependence of the magnetization critical current density $J_{cm}$

Figure 3 shows the hysteresis loops taken at 10, 40, and 75 K with $H\|c$ for the three samples. Several observations are notable from hysteresis loops performed in the temperature range 7–80 K.

(i) The width of the hysteresis loops increases with Y 2:1:1 phase concentration except for temperatures near 40 K for which the difference between Y 1.5 and Y 1.0 is negligible. However, because the value of magnetization

critical current density $J_{cm}$ depends upon both $\Delta M$ and the sample dimension, the magnitude of $J_{cm}$ for these samples does scale with the amount of Y 2:1:1 phase.

(ii) Figure 2 shows $M$ to have a larger magnitude for $H\|c$ than for $H\perp c$. After accounting for the effective supercurrent-carrying dimensions in these orientations, $J_{cm}$'s derived from the two hysteresis loops are significantly different. This anisotropy implies $J_{cm}$ circulating in the $ab$ plane with $H\|c$ is much higher than that for $H\perp c$. In the latter case, $J_{cm}$ has components in the $ab$ plane and along the $c$ axis, respectively. $J_{cm}(\|c)$ is much smaller than $J_{cm}(\|ab)$.

(iii) "Butterfly" or "fishtail" hysteresis loops were observed in Y 1.5 and Y 1.8 when $T > 40-50$ K. This is more evident in Y 1.8 than in Y 1.5. This phenomenon has been shown to be associated with local regions of oxygen deficiency in Y 1:2:3 crystals.[13,55] Since oxygen deficiency lowers $T_c$, these regions may be driven normal at large fields and high temperatures where the matrix is still superconducting. Thus new pinning centers are generated as the field is increased, causing $J_{cm}(B)$ to be an increasing function of $B$. This same mechanism may be operative for any defect structure that locally depresses $T_c$ and has been observed for a variety of precipitates in conventional superconductors.[56] Therefore, defects associated with Y 2:1:1-phase particles may be responsible for

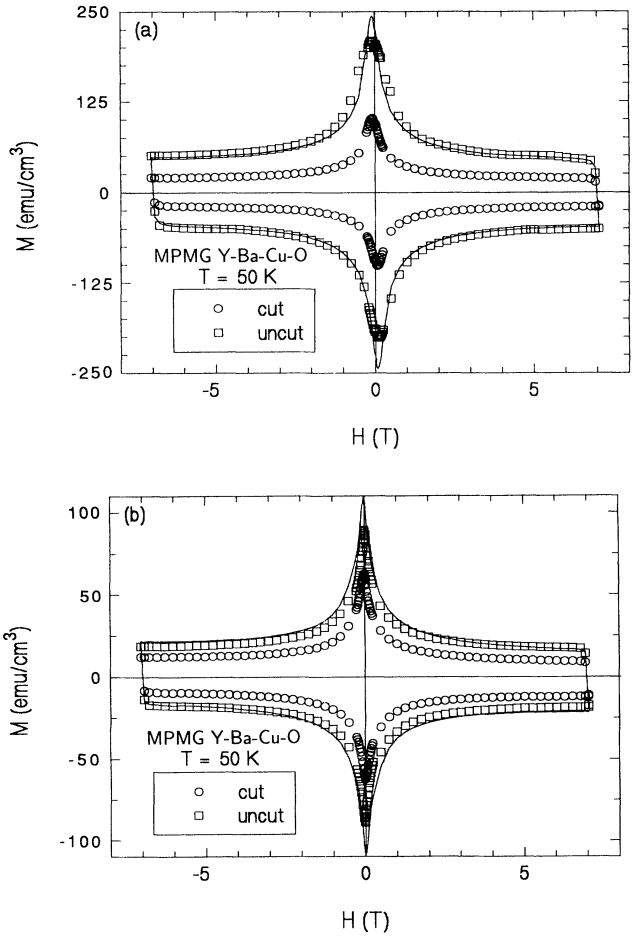


FIG. 2. Magnetization hysteresis loops with the field applied (a) parallel and (b) perpendicular to the $c$ axis of the sample. The sample was measured before and after being cut approximately in half. The solid line was obtained from data taken for the cut piece by scaling with the change in sample dimension in accordance with the Bean model expression, Eq. (9).

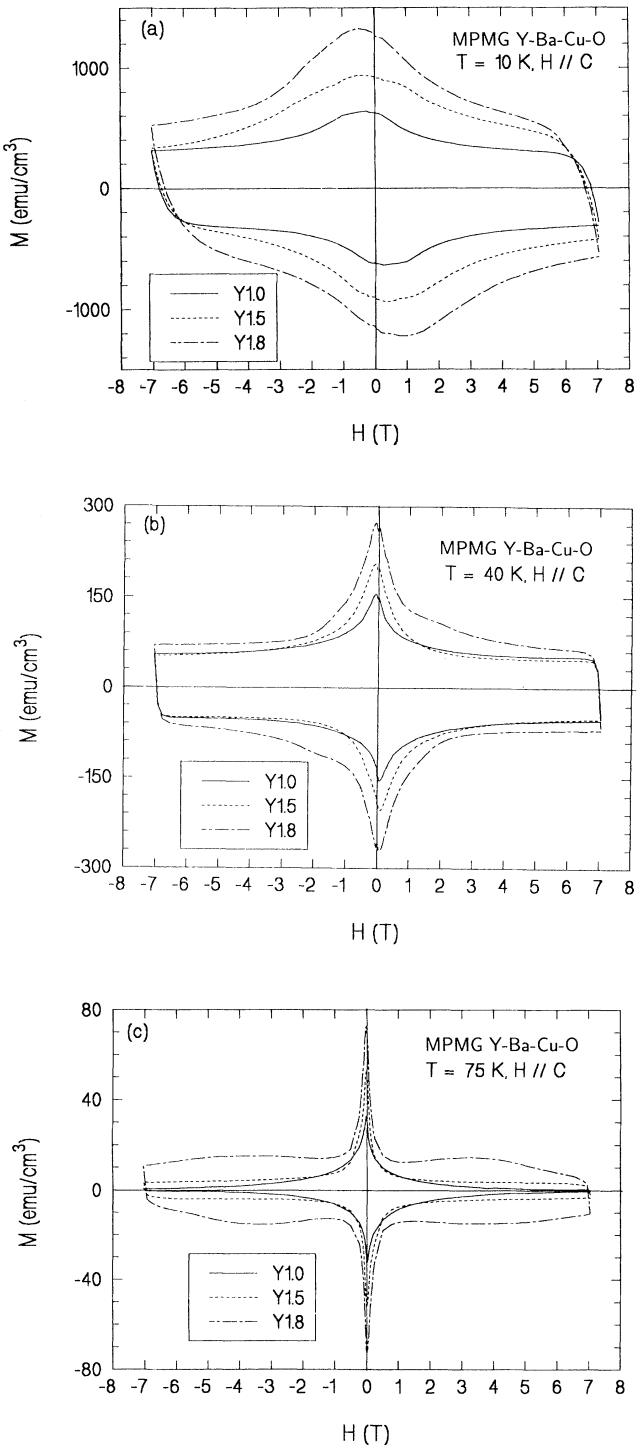


FIG. 3. Comparison of the magnetic hysteresis loops for Y 1.0, Y 1.5, and Y 1.8 samples at (a) 10 K, (b) 40 K, and (c) 75 K.

this observation.

(iv) Hysteresis loops show a weak-field dependence even at $T > 60-70$ K in fields up to 7 T, which indicates strong pinning in these MPMG-processed samples. For Y 1.8, the hysteresis loop at 80 K still exhibits significant irreversibility at the highest measured field (7 T).

Using Eq. (9) with $M_{irr}$ determined by $\Delta M$, $J_{cm}$'s were calculated. As mentioned earlier (also see Fig. 2), these MPMG-processed samples show no evidence of being weak linked. Therefore, we use the sample dimensions to derive $J_{cm}$. Figures 4 and 5 summarize the field and temperature dependence of $J_{cm}$, respectively, in which the following occurs.

(i) The magnitude of $J_{cm}$'s increases with the concentration of Y 2:1:1 inclusions. $J_{cm}$'s of $10^4$ A/cm$^2$ are attained at 70 K and 5 T except for the Y 1.0 sample (see Fig. 4).

(ii) At high fields (i.e., $H > 2$ T) and high temperature (see $T \geq 70$ K) in Fig. 5, the temperature (i.e., at constant field) and field dependence (i.e., at constant temperature) of $J_{cm}$ becomes weaker with increasing concentration of Y 2:1:1 inclusions. This effect is less pronounced at low temperatures. This suggests that the pinning of the nonsuperconducting Y 2:1:1 phase in Y-Ba-Cu-O becomes more important at elevated temperature and field.

(iii) As illustrated in Fig. 5, $J_{cm}$ approximately follows an exponential dependence of temperature for $T < 60$ K, and drops more rapidly when $T$ is close to $T_c$. Similar observations for $J_{cm} \propto \exp(-cT)$ (where $c$ is a constant) were also previously reported.[57,58] This behavior is different from a power-law relation for $J_c(T)$, which was suggested for $J_c$ limited by flux creep in an early model for this phenomenon.[59] The observed magnitude and exponential temperature dependence in $J_{cm}(T)$ are similar to the results of Yeh *et al.*[60] for Y-Ba-Cu-O powder samples.

(iv) $J_{cm}$ values reported here represent intergranular values. However, due to thermally activated flux creep and the finite time required for measurement of the initial $M$, we never actually measure $J_{cm}$. Instead, we measure a

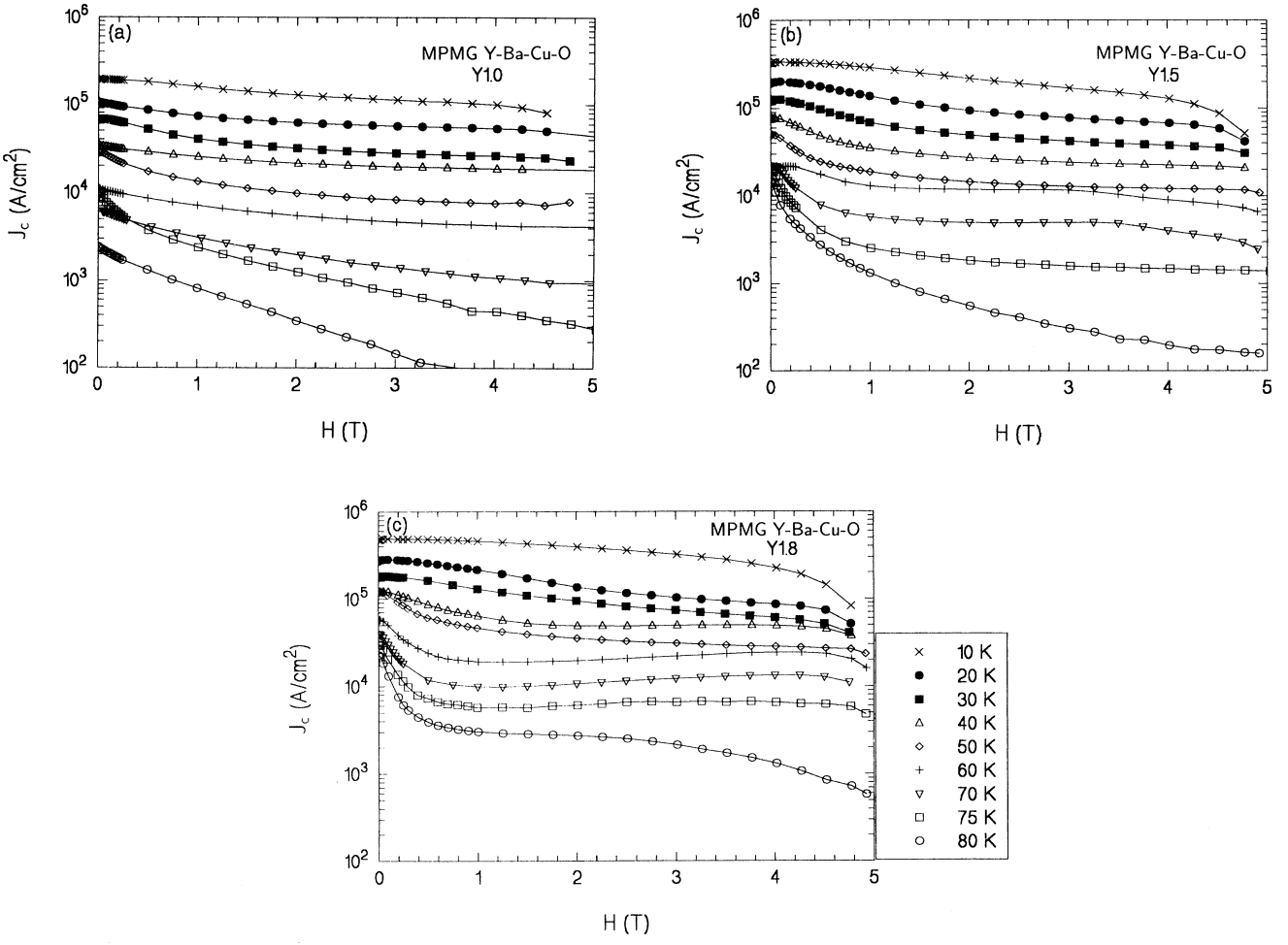


FIG. 4. Field dependence of the magnetization critical current densities derived from the magnetic hysteresis ($H \| c$ axis) for (a) Y 1.0, (b) Y 1.5, and (c) Y 1.8 samples. Notice that a peak or shoulder exists in the curves for $T > 40$ K and $H > 2$ T in Y 1.5 and Y 1.8. These features are caused by field- and temperature-driven flux pinning associated with the defect-induced reduced $T_c$ regions. Especially in Y 1.8, it is very easy to observe a much weaker field dependence of $J_{cm}$.

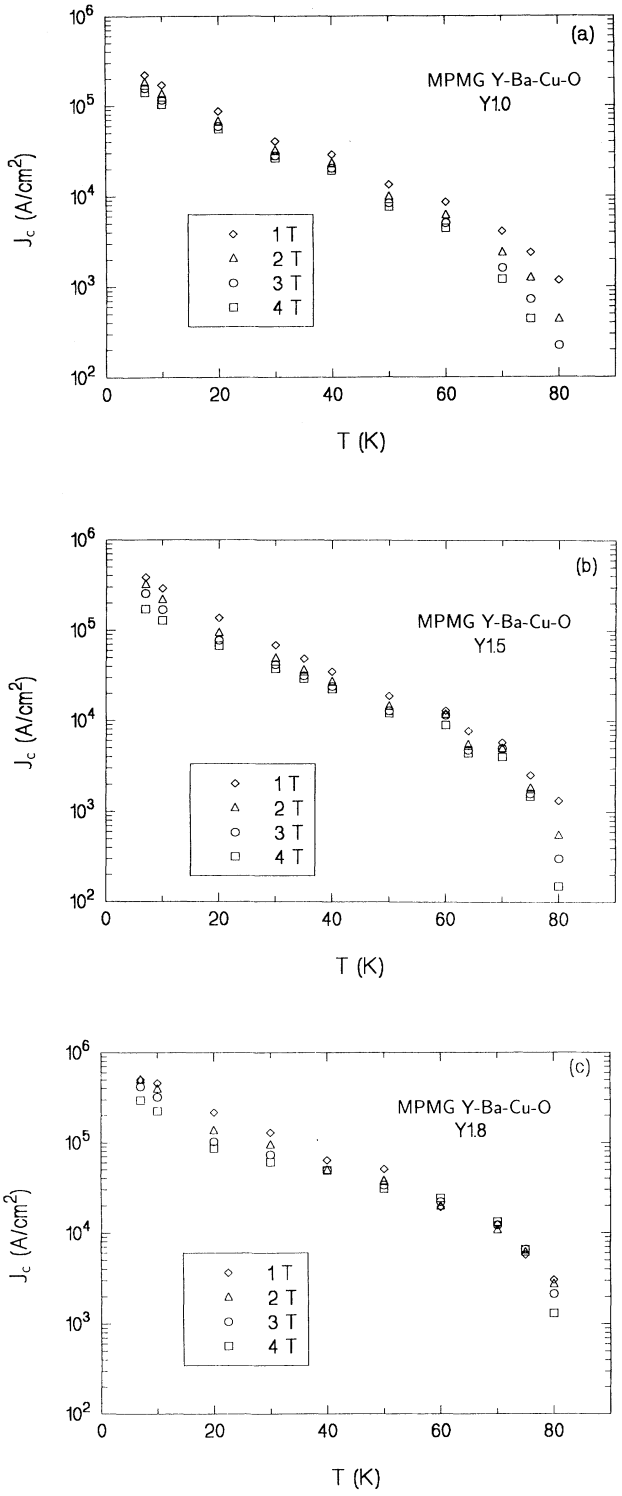


FIG. 5. Temperature dependence of the magnetization critical current densities derived from the magnetic hysteresis ($H \| c$ axis) for (a) Y 1.0, (b) Y 1.5, and (c) Y 1.8 samples. An exponential relation $J_{cm} \propto \exp(-cT)$ describes approximately the $J_{cm}(T)$ curves for $T < 60$ K. At higher temperatures, the rapid drop of $J_{cm}$ with $T$ is sufficiently reduced for increasing Y 2:1:1 concentrations.

relaxed value resulting from rapid creep away from the critical state. The higher voltage sensitivity in a magnetic measurement compared to transport methods also leads to values of $J_{cm}$ smaller than $J_{ct}$ (transport critical current density).[61]

(v) Notice that the temperature dependence $J_{cm}(T)$, at fields well below 1 T, is not as dramatic as usually observed in granular high-$T_c$ bulk superconductors. This observation, accompanied by the weak-field dependence of $J_{cm}$ in the high-field regime, reflects both strong intergranular coupling and intragranular pinning in the MPMG-processed material.

### C. Magnetic relaxation and the $U_{\text{eff}}(J)$ relation

Figure 6 shows a linear dependence of magnetization upon the logarithm of time at 3 T for different temperatures demonstrating the usual relaxation of the pinned mixed state in HTSC's. In order to study the effects of temperature and Y 2:1:1 concentration on flux creep, the

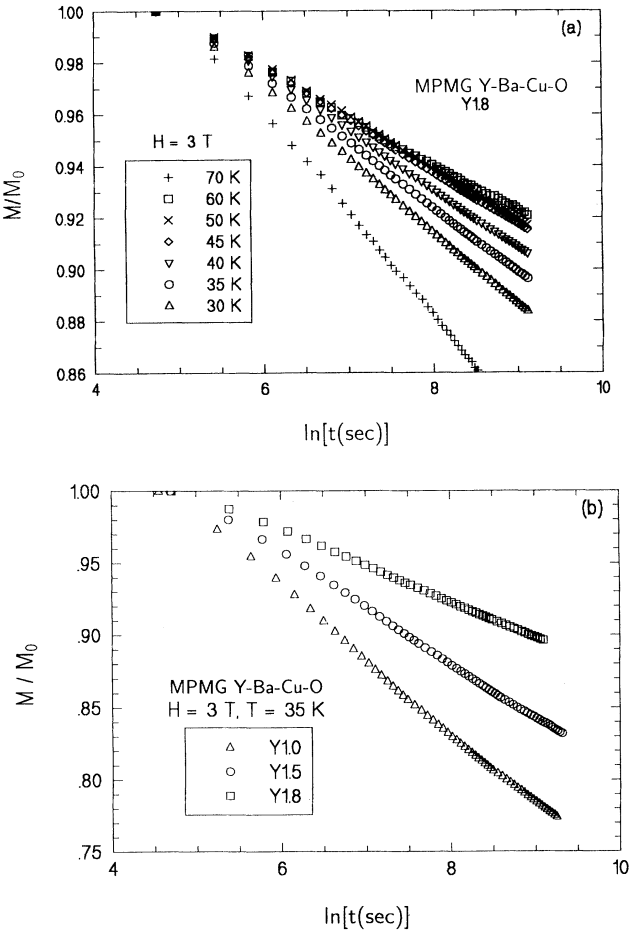


FIG. 6. Magnetic relaxation measured at 3 T and various temperatures on the MPMG-processed Y 1:2:3 samples showing a quasilinear dependence on the logarithm of time. (a) shows the data for the Y 1.8 sample at various temperatures, and (b) the data obtained at 35 K from the Y 1.0,Y 1.5, and Y 1.8 samples for comparison. In (b) the decay of $M/M_0$ with time is reduced with increasing Y 2:1:1 concentration.

magnetization $M$ is normalized to the initial magnetization $M_0$. It is clearly seen that the slope of $M/M_0$ versus $\ln t$ decreases slightly with temperature except for 70 K [see Fig. 6(a)]. This result implies a faster normalized relaxation rate $S=-(1/M_0)(dM/d\ln t)$ at 70 K, which is consistent with $S$ diverging at $T>60$ K as reported in previous work.[43] The addition of Y 2:1:1 inclusions to Y-Ba-Cu-O also decreases the relaxation rate [see Fig. 6(b)].

To extract the effective pinning energy $U_{\rm eff}$ from experimental relaxation data, we measured $M(t)$ for each sample at fixed fields (1, 2, 3, and 4 T) and temperatures (5–80 K). The measured $M$ (emu/cm$^3$) was converted to current density $J$ (A/cm$^2$) using the procedure described above [see Eq. (9)]. The initial magnetization $M_0$ was compared with values on a separately measured hysteresis loop at the same temperature and magnetic field to assure that no flux jump or misalignment had occurred. Using Eq. (5), we select the constant $C=\ln[Ba\omega_0/\pi d]$ to achieve continuity of $U_{\rm eff}(J)$ for $T\le 15$ K, where we expect the intrinsic temperature dependence of $U_{\rm eff}$ to be negligible. Table I lists the values of $C$ for each field; $C$ increases slightly with applied field and is not strongly sample dependent. We account for these results as follows.

(i) According to the definition of $C$, an increase in the applied magnetic field (and hence the magnetic induction $B$) should lead to a higher $C$ value. Table I shows a change in $C$ from 14 to 16 (e.g., compare 2 T and 3 T in Y 1.0 and Y 1.5).

(ii) At a constant magnetic field the largest value of $C$ is obtained for Y 1.8, while those for Y 1.0 and Y 1.5 are equal. Because the Y 2:1:1 concentration increases from Y 1.0 and Y 1.5 to Y 1.8, the change in $C$ cannot unambiguously be attributed to the presence of Y 2:1:1 inclusions. Other defects including removing oxygen from chain sites in Y-Ba-Cu-O have been shown to result in larger $C$ values (changed from 15 to 18).[62] Nevertheless, the dimensions for our three samples vary only by $\sim 15\%$, and the near sample independence of $C$ indicates the rough constancy of $a\omega_0$.

(iii) Another interpretation of the value of $C$ comes from a consideration of flux-flow resistivity. Employing the Bardeen-Stephen model of flux flow, van der Beek *et al.*[63] derived an expression for the constant $C$:

$$C=\ln\left[\frac{2\rho_{fs}J_s}{\mu_0 d}\right], \tag{13}$$

where $J_s\propto M-M_{eq}$, $\rho_{fs}\approx\rho_n B/B_{c2}$ is the flux-flow resistivity ($\rho_n$ is the normal-state resistivity), and the subscript "$s$" denotes variables evaluated at the sample surface. Substituting the expression for $\rho_f$ into Eq. (13) yields

$$C=\ln\left[\frac{2\rho_{fs}J_s}{\mu_0 d}\right]\approx\ln\left[\frac{2\rho_n BJ}{B_{c2}\mu_0 d}\right].$$

Comparing MPMG-processed Y-Ba-Cu-O with bulk Bi-Sr-Ca-Cu-O for $H\|c$, the former has slightly higher $J$ and $B_{c2}$ and similar $\rho_{n,ab}$ ($\sim 10\ \mu\Omega$ cm). The most important variable for determining $C$ values thus turns out to be the sample dimension which can vary over several orders of magnitude from grain sizes ($\sim\mu$m) to typical sample sizes ($\sim$mm). With other variables kept constant, a smaller sample results in higher $C$ values.

(iv) The three samples studied in this work have similar transverse dimensions. If we adopt the definition of $C$ in Eq. (13), the main factor that remains to determine the constant $C$ is $J$. Thus, for instance, at a given magnetic field, Y 1.8 should and does have the highest $C$, which is consistent with its highest $J$ among these samples.

Figure 7 shows the curves of $U_{\rm eff}$ calculated from $M(t)$ data versus $J$. The applied field, the temperature range of measurement, and the sample name are indicated. Each segment represents the data collected at a given temperature. The lowest temperature (i.e., 5 K) is located on the high-$J$ side. With increasing temperature, the $J$ values decrease and $U_{\rm eff}$'s gradually increase. Table II lists the measurement temperatures and magnetic fields employed in this work. We found the value of $U_{\rm eff}(J)$ to increase with the concentration of Y 2:1:1 inclusions. From Fig. 7, we see that before scaling with $G(T)$, the high-temperature data points fall below the smooth curve that can be extended from the low-temperature regime. Temperature scaling is determined as follows.

(i) Beginning with the 15-K data set, each isothermal set taken at $T>15$ K is multiplied by a scaling factor so that it forms a continuous curve with the data sets recorded at the two adjacent lower temperatures. The high-temperature data points are thus moved upwards to insure continuity with the curve extrapolated from the low-temperature data.

(ii) The scaling function $G(T)$ is determined directly from these multiplicative factors chosen for each temperature. A less desirable alternative is to pick a model function for $G(T)$. We have found that several hypothetical expressions for $G(T)$ do not completely account for the implicit temperature dependence over a wide range of $J$ (or $T$).

A plot of $U_{\rm eff}(J)/kG(T)$ versus $J$ on a double logarithmic scale is shown in Fig. 8, and indicates a significant field dependence for $U_{\rm eff}(J)$. For 3- and 4-T data, the curves obtained from the Y 1.8 sample begin to bend upward at $T\sim 45$ K and above. The data of Fig. 8 have been regrouped and plotted in Fig. 9 to illustrate the effect of field on the effective pinning energy for each sample. As can be seen, the lower-field data exhibit a higher $U_{\rm eff}$ resulting from a higher absolute value of

TABLE I. Constants used to fit the temperature dependence of $U_{\rm eff}$. The constant $C=\ln(Ba\omega_0/\pi d)$ was derived from fitting the $U_{\rm eff}$ versus $J$ data for $T\le 15$ K to a smooth curve as described in the text.

| $H$ (T) | Y 1.0 | Y 1.5 | Y 1.8 |
|---|---|---|---|
| 1 | 14 | 14 | 14 |
| 2 | 14 | 14 | 14 |
| 3 | 16 | 16 | 17 |
| 4 | 16 | 16 | 17 |

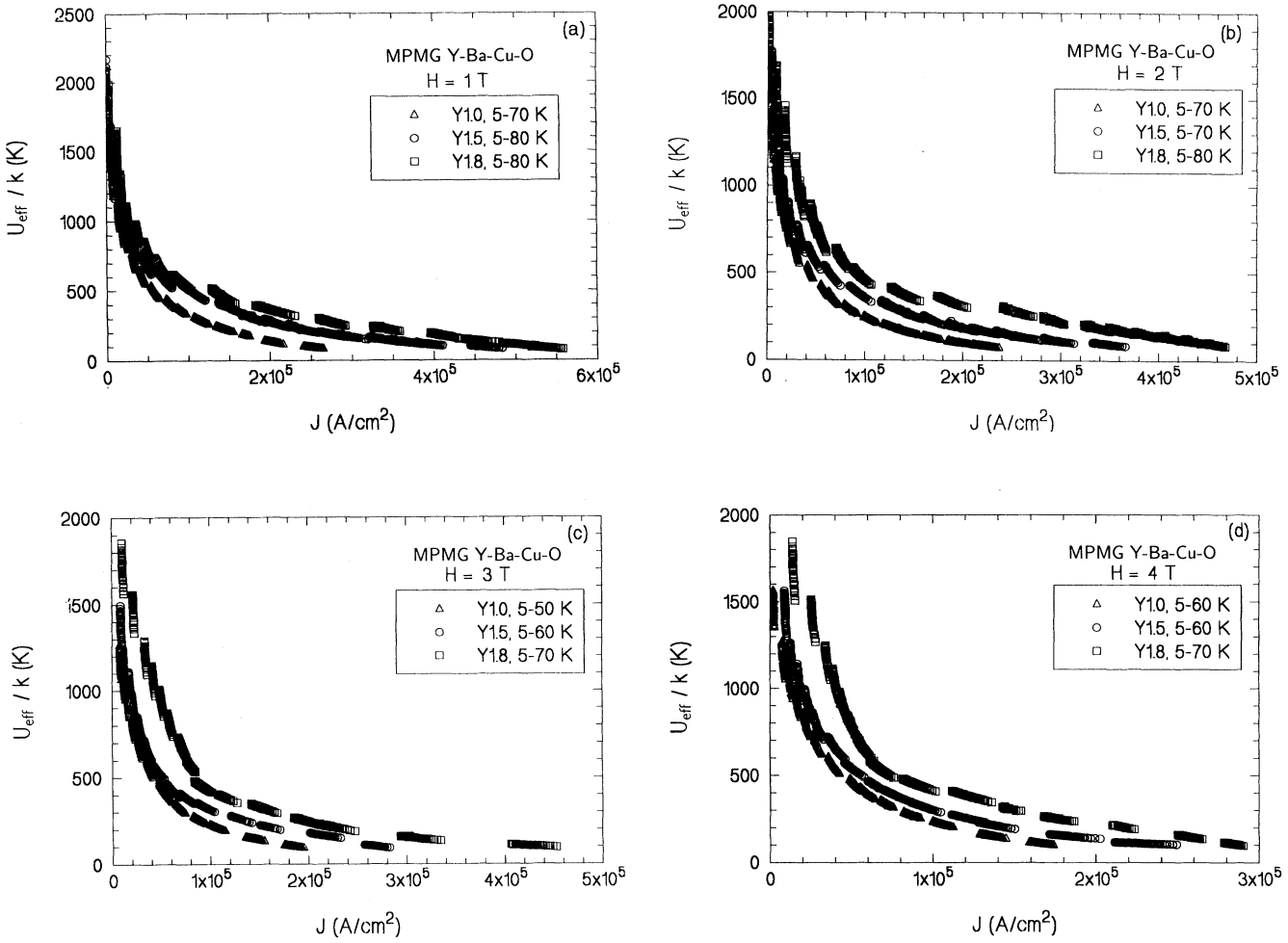


FIG. 7. Fits of the data to $U_{\text{eff}}/k$ versus current density $J$ for Y 1.0, Y 1.5, and Y 1.8 at magnetic fields of (a) 1 T, (b) 2 T, (c) 3 T, and (d) 4 T, respectively.

TABLE II. The temperatures (K) and magnetic fields (T) at which the measurement of magnetic relaxation was performed.

| | |
|---|---|
| Y 1.0 | 1 T: 5, 7, 10, 12, 15, 18, 20, 25, 30, 35, 40, 45, 50, 60, 70 |
| | 2 T: 5, 6, 7, 9, 10, 12, 15, 18, 20, 25, 30, 35, 40, 45, 50, 60, 70 |
| | 3 T: 5, 7, 10, 12, 15, 18, 20, 25, 30, 35, 40, 45, 50 |
| | 4 T: 5, 7, 10, 12, 15, 18, 20, 25, 30, 35, 40, 45, 50, 60 |
| Y 1.5 | 1 T: 5, 6, 7, 8, 9, 10, 12, 14, 16, 20, 25, 30, 35, 40, 45, 50, 60, 70, 80 |
| | 2 T: 5, 6, 7, 8, 9, 10, 12, 14, 16, 20, 25, 30, 35, 40, 45, 50, 60, 70 |
| | 3 T: 5, 8, 10, 12, 15, 18, 20, 25, 30, 35, 40, 45, 50, 60 |
| | 4 T: 5, 7, 10, 12, 15, 18, 20, 25, 30, 35, 40, 45, 50, 60 |
| Y 1.8 | 1 T: 5, 6, 8, 10, 12, 15, 20, 25, 30, 35, 40, 45, 50, 60, 70, 80 |
| | 2 T: 5, 6, 7, 8, 9, 10, 12, 15, 18, 20, 25, 30, 35, 40, 45, 50, 60, 70, 80 |
| | 3 T: 5, 7, 10, 12, 15, 18, 20, 25, 30, 35, 40, 45, 50, 60, 70 |
| | 4 T: 5, 7, 10, 12, 15, 18, 20, 25, 30, 35, 40, 45, 50, 60, 70 |

$\ln(dM/dt)$ at a given value of $J$. Again, in Y 1.8, the 3- and 4-T data bend upward in the high-temperature region (or at the low-$J$ side). As illustrated in Fig. 10, the $U_{\text{eff}}(J)/kG(T)$ curve at 3 T crosses the 2-T curve showing higher effective pinning energies. Also, the 4-T curve merges with the 2-T curve. This is consistent with the hysteresis loops observed in the Y 1.8 sample (which are not as significant in Y 1.5) and clearly indicates that the peak in the loop is associated with an enhanced activation energy. Because of the superposition of pinning of the Y 2:1:1 inclusions and pinning due to unknown defect regions, which become normal at high temperature and magnetic field, the effective pinning energy $U_{\text{eff}}$ is shifted to higher values.

Determination of the functional dependence of the numerically determined $G(T)$ by curve fitting was made using several trial expressions for $G(T)$ of the forms $(1-T/T_x)^m$ and $[1-(T/T_x)^n]^m$, where $T_x$ can be $T_c$, $T_{\text{irr}}$, or be treated as a fitting parameter. The choice of these functional forms is often based on the general expressions for the temperature dependence of $H_c(T)$, $\lambda(T)$, and $\xi(T)$ derived from the Ginzburg-Landau theories. $G(T)=(1-T/T_c)^{3/2}$ (Refs. 48, 59, and 64), $[1-(T/T_x)^2]$ (Ref. 43), and $[1-(T/T_x)^2]^{3/2}$ (Ref. 62) have been suggested for a variety of systems. It was found in the present study that adequate fits to the form $G(T)=[1-(T/T_{\text{irr}})^2]^m$ could be obtained with $m$ as a fitting parameter. The fits and the $m$ values are shown in Fig. 11 and listed in Table III, respectively. As is evident in Fig. 11, only for the Y 1.0 sample could a consistent fit to the temperature dependence $G(T)$ be obtained with a narrow range of $m$ values ($2.0 \leq m \leq 3.2$) for all fields. For the other samples containing large Y 2:1:1 fractions, the fits are a poor description of the data, particularly for the Y 1.8 sample. This breakdown of temperature scaling with forms derived from thermodynamic variables is to be expected from the appearance of butterfly hysteresis loops and the implied anomalous temperature and field dependence of pinning activation energies. We have also found the following.

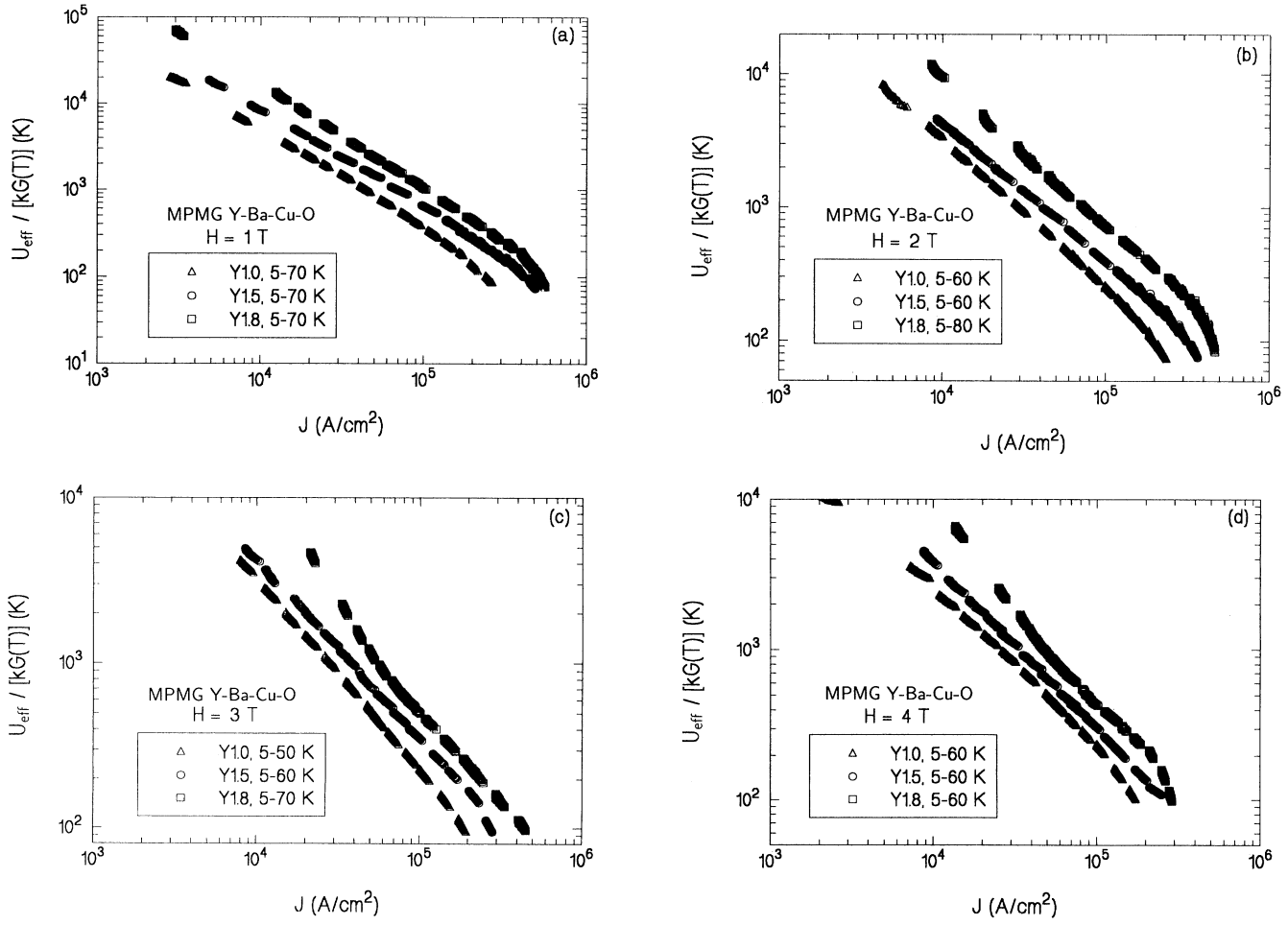


FIG. 8. Fits of the data to $U_{\text{eff}}/kG(T)$ versus current density $J$ for Y 1.0, Y 1.5, and Y 1.8 at magnetic fields of (a) 1 T, (b) 2 T, (c) 3 T, and (d) 4 T, respectively. Notice that the 3- and 4-T curves for Y 1.8 bend upward at low $J$, which is caused by the pinning due to low-$T_c$ phases added to the pinning from Y 2:1:1 inclusions.

(i) $T_x = T_{irr}$ indicates the important role played by the irreversibility line, which has been proposed as a transition between vortex-glass and vortex-liquid phases.[10] As $J$ approaches zero, $U_{eff}(J)/kG(T)$ grows without limit. This is a signature of the vortex-glass state that exhibits diverging energy barriers between metastable states and $\rho = 0$. In these measurements this limit is approached as $T$ nears $T_{irr}$ from below. As a consequence, choice of $T_x = T_c$ is inconsistent with the observed experimental data. Scaling of activation energies with $T_{irr}$ is a reflection of the importance of thermal fluctuations even at lower temperatures.

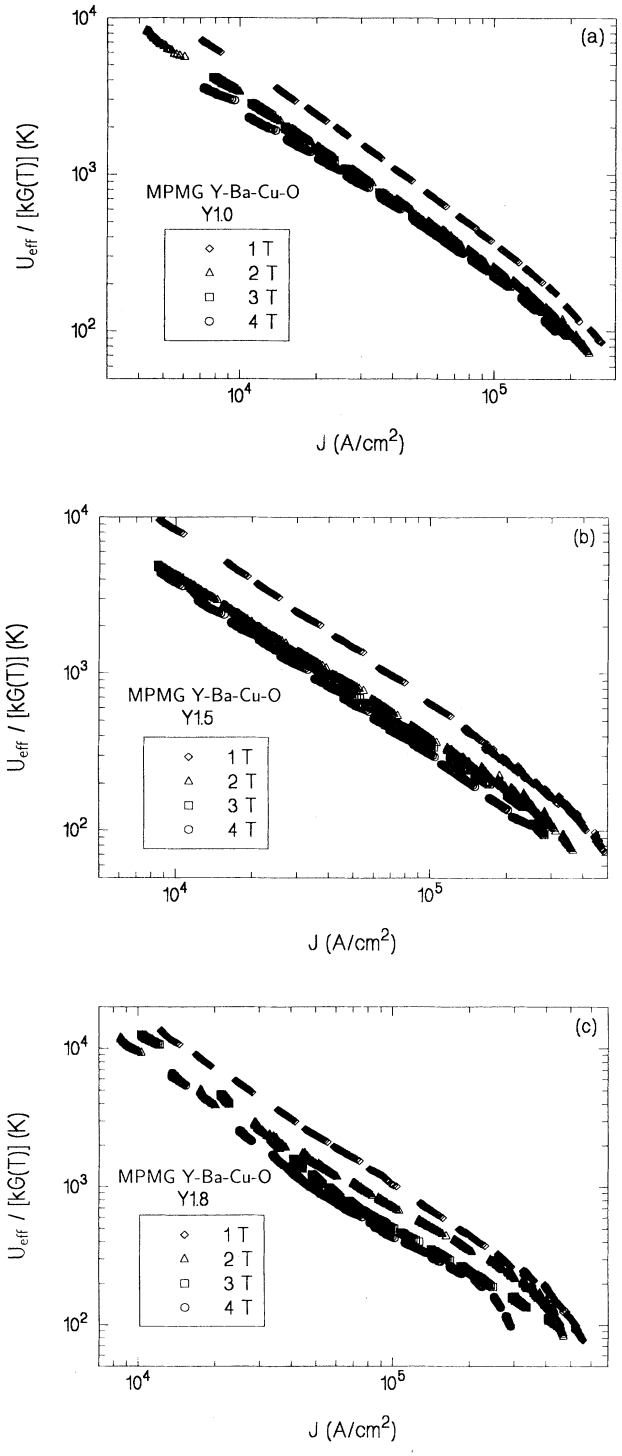


FIG. 9. The curves of $U_{eff}/kG(T)$ versus $J$ replotted from Fig. 8 for each sample, namely, (a) Y 1.0, (b) Y 1.5, and (c) Y 1.8 to show more clearly the field dependence.

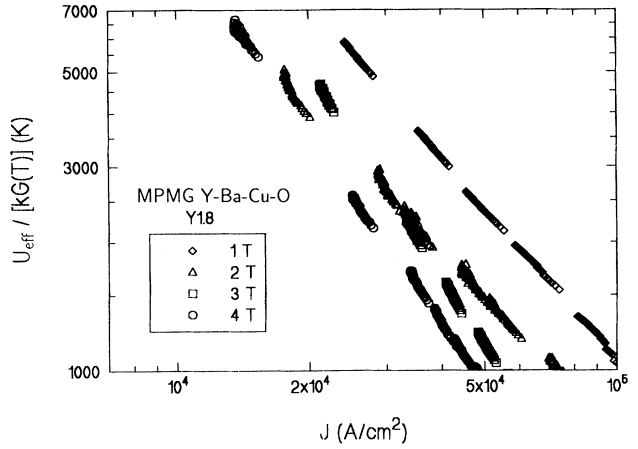


FIG. 10. Expanded plot of Fig. 9(c) in the low-$J$ (high-$T$) regime to show clearly that the 3- and 4-T curves begin to bend upward at temperatures around 45 K and above. The 3-T curve actually intersects the 2-T curve.

(ii) The field dependence of $G(T)$ becomes stronger as the Y 2:1:1 concentration is increased (i.e., from Y 1.0 to Y 1.8), but it does not scale well with the concentration of Y 2:1:1 inclusions if we compare Y 1.0 versus Y 1.5 with Y 1.5 versus Y 1.8. The very different shape in the $G(T)$ data for Y 1.8 at 3 and 4 T can be attributed to the combined pinning effect due to Y 2:1:1 inclusions and the defects whose pinning strength increases with the magnetic field. This also can be seen by comparing the $m$ values in Table III among the samples. Again, temperature scaling of the Y 1.8 sample is expected to be abnormal because of the unusual temperature and field dependence manifested in the butterfly shape of the hysteresis curves.

To determine the functional dependence of $U_{eff}(J)$ on magnetic field, the data at all fields were scaled by the factor $H^n$, where the $n$ value was selected to make the curves at different fields coincide. The results are shown in Table IV. We have found that a slight increase in $n$ occurs as the concentration of Y 2:1:1 inclusions is increased. However, because of the $J$ dependence of flux

TABLE III. The $m$ values in $G(T) = [1-(T/T_x)^2]^m$ determined from least-squares curve fitting the temperature dependence of $U_{eff}$, where $T_x \cong T_{irr}$.

| $H$ (T) | Y 1.0 | Y 1.5 | Y 1.8 |
|---|---|---|---|
| 1 | 3.184 | 3.675 | 4.553 |
| 2 | 2.862 | 2.657 | 2.652 |
| 3 | 2.614 | 2.346 | 1.208 |
| 4 | 1.961 | 1.667 | 0.783 |

TABLE IV. The $n$ values used to scale the field dependence $H^n$ of $U_{eff}$.

| Y 1.0 | Y 1.5 | Y 1.8 |
|---|---|---|
| 0.46±0.02 | 0.57±0.01 | 0.61±0.03 |

pinning mechanisms, a single value of $n$ cannot be employed properly over the entire range of $J$. This deviation from scaling is obvious in the low-$J$ regime for Y 1.8 as shown in Fig. 12. Although Y 1.5 probably also has similar field-induced pinning centers, the resulting effect is less noticeable. The average $n$ value obtained from this work for three MPMG-processed samples is around 0.5, which indicates a weaker field dependence than $n=1$ observed for several single-crystal samples. For instance, $n=0.5$, 1, and 2 have been reported.[12,48,65–67] The value $n=0.5$, similar to our results, has been suggested for flux pinning dominated by twin planes. Though twin planes are also observed in our samples, their density is independent of the presence of Y 2:1:1 inclusions. Therefore, the $n$ values obtained for this work are believed to be mainly determined by the flux pinning from Y 2:1:1 inclusions. Since twin planes have larger longitudinal dimensions than the Y 2:1:1 particle sizes, if the FLL is very rigid and the vortices are parallel to twin planes, strong flux pinning is expected to result. On the other hand, our samples have a very homogeneous distribution of Y 2:1:1 inclusions. They can provide collective flux pinning for a soft FLL. This leads to a weak-field dependence of $U_{eff}(J)$.

As shown in Fig. 12, the $J$ dependence of $U_{eff}H^n/kG(T)$ for the three samples can be broken into two power-law regimes following Eq. (11). In this figure, solid lines, denoting exponents (i.e., $\mu$) of $\frac{7}{9}$ (for bundle sizes $R_b > \lambda_L$) and $\frac{3}{2}$ (for $R_b \ll \lambda_L$), are those predicted by the collective flux-creep model for a 3D system.[9] The results in the high-$J$ regime (or low-$T$) agree quantitatively with the model. At low $J$ our exponent is $\frac{9}{10}$, which is slightly larger than the predicted $\frac{7}{9}$ value. Similar deviation from theoretical results was also reported in a field-aligned $YBa_2Cu_3O_{6.8}$ sample,[62] in which excess oxygen defects were demonstrated to reduce $U_{eff}(J)$. Figure 12 also shows that a diverging $U_{eff}(J)$ in the low-$J$ regime which is consistent with the existence of a vortex-glass state.[10] However, the $\mu=\frac{1}{7}$ exponent of the single-vortex regime has not been able to be demonstrated in this work; it was not possible to perform measurements in the range of $J \sim J_c$ where this regime is expected to occur. In summary, the experimentally observed functional form of $U_{eff}(J,T,H)$ can be modeled by

$$U_{eff}(J,T,H)=\frac{U_1}{H^n}\left[1-\left[\frac{T}{T_{irr}}\right]^2\right]^m\left[\frac{J_i}{J}\right]^\mu, \qquad (14)$$

where $U_1$ contains all numerical factors, $J_i$ defines the boundaries between different current density regimes which depend on flux bundle sizes, the value of $m$ depends on the applied field, and the Y 2:1:1 content, $\mu$ is the exponent either predicted from the collective flux-creep model or obtained from $U_{eff}(J)$ curves, and $n$ depends on the Y 2:1:1 concentration. However, only for the Y 1.0 sample does this form provide a consistent description with a narrow range of the parameters $n$ and $m$ for all fields and temperatures.

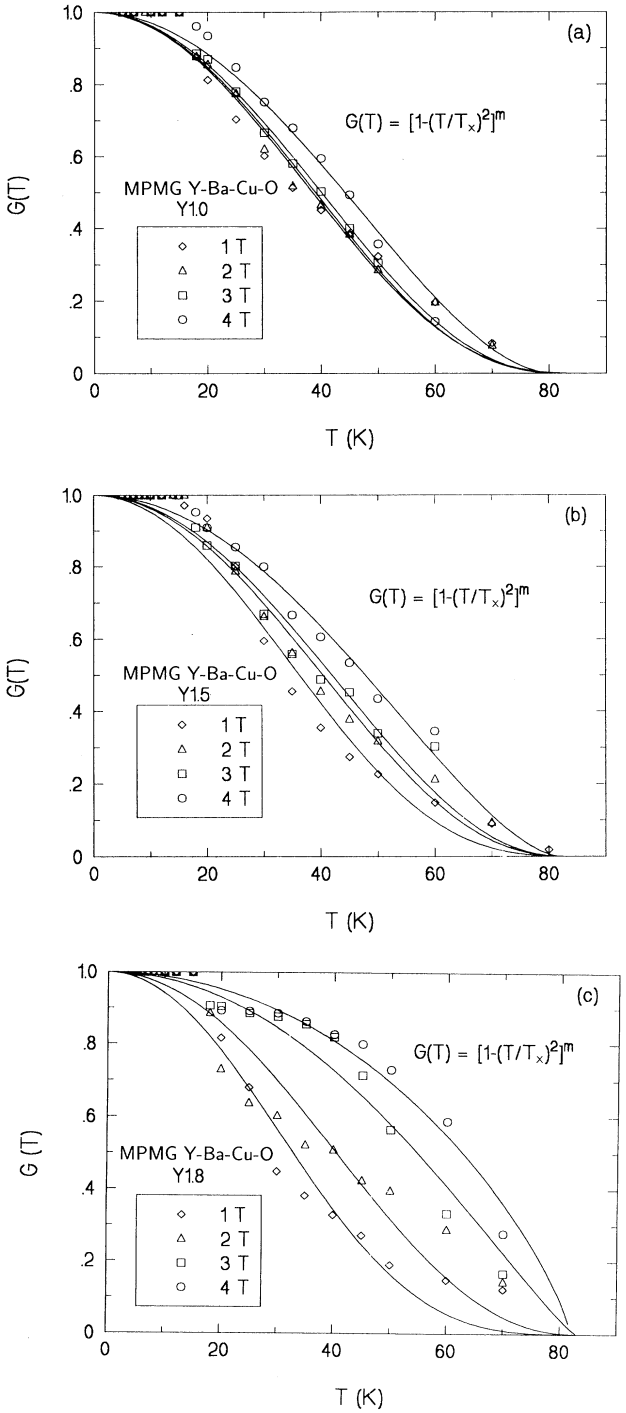


FIG. 11. The numerically derived $G(T)$ values from fitting the temperature dependence of $U_{eff}(J)$ at $H=1$, 2, 3, and 4 T for (a) Y 1.0, (b) Y 1.5, and (c) Y 1.8. The solid lines were obtained from least-squares fitting of the functional expression $G(T)=[1-(T/T_x)^2]^m$, where the $m$ values are listed in Table III.

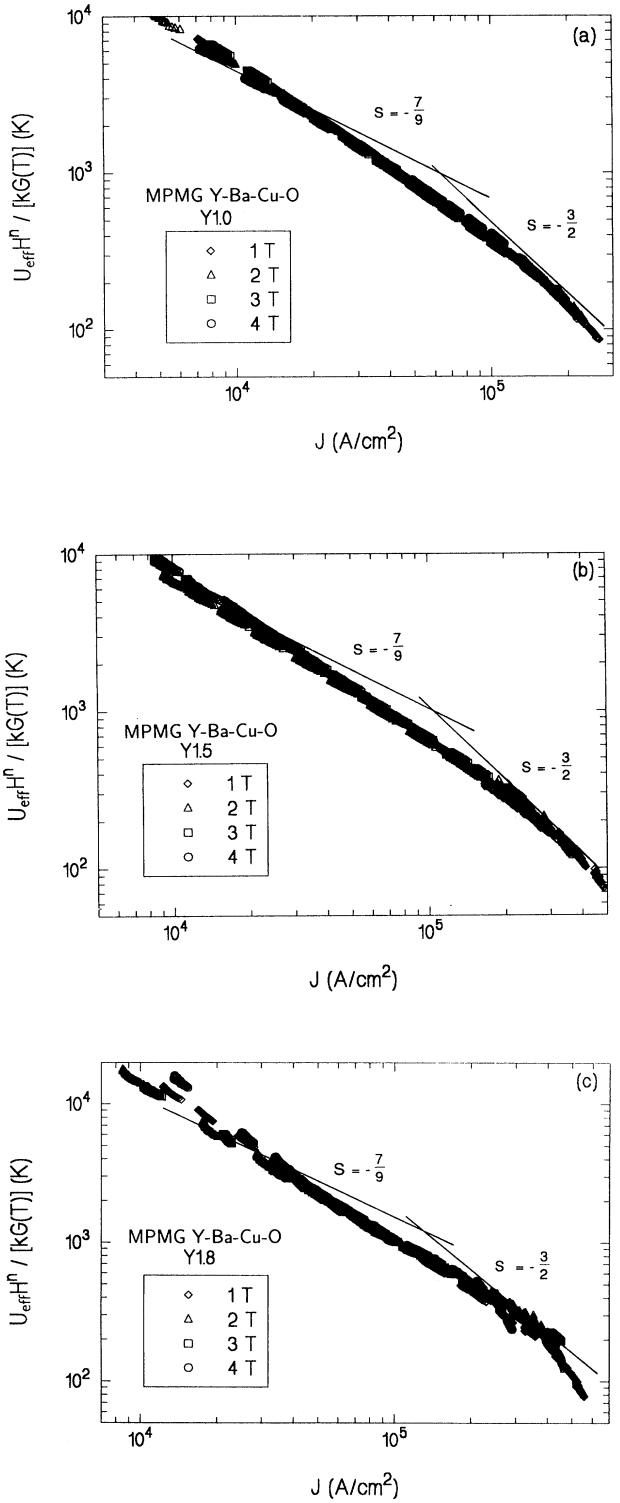


FIG. 12. Fits of $U_{\text{eff}}H^n/kG(T)$ versus $J$ at $H=1$, 2, 3, and 4 T for (a) Y 1.0, (b) Y 1.5, and (c) Y 1.8. The $n$ values are listed in Table IV. Notice that for these samples, the curves can be separated into two linear regions, which is consistent with the collective flux-creep theory. The solid lines are the slopes of $-\frac{7}{9}$ and $-\frac{3}{2}$ predicted by the theory and are drawn for comparison.

### D. Temperature scaling of $U_{\text{eff}}[J/J_i(T)]$

Determination of the dependence of activation energies for flux motion on current density and temperature from magnetic relaxation is complicated by the strong correlation between various ranges of $J$ and $T$ accessible in the measurement. At low temperatures, $J$ is restricted to be near $J_c$ where sufficiently low values of $U_{\text{eff}}(J)/kT$ are obtained to establish measurable rates of relaxation. At higher temperature, rapid relaxation away from the critical state occurs until a barrier height is established that reduces the relaxation rate at a "persistent" value of $J \ll J_c$. In general, $U_{\text{eff}}(J,T)/kT \approx \ln(t/\tau)$, where $\tau$ is a time constant that depends upon sample dimensions.[49] This general relation determines a window of $J$ values accessible at a given temperature on the time scale $t$. Thus, the major effect of changing $T$ is to vary the range of current densities observed during the relaxation.

Although we have chosen above to account for the remaining implicit temperature dependence of $U_{\text{eff}}(J,T)$, with the scaling function $G(T)$, this is not a unique formulation. In particular, in vortex-glass and collective creep models $U_{\text{eff}}(J,T)=G(T)F[J/J_i(T)]$, where $J_i(T)$ is a scaling function that in the single-vortex (high-$J$) re-

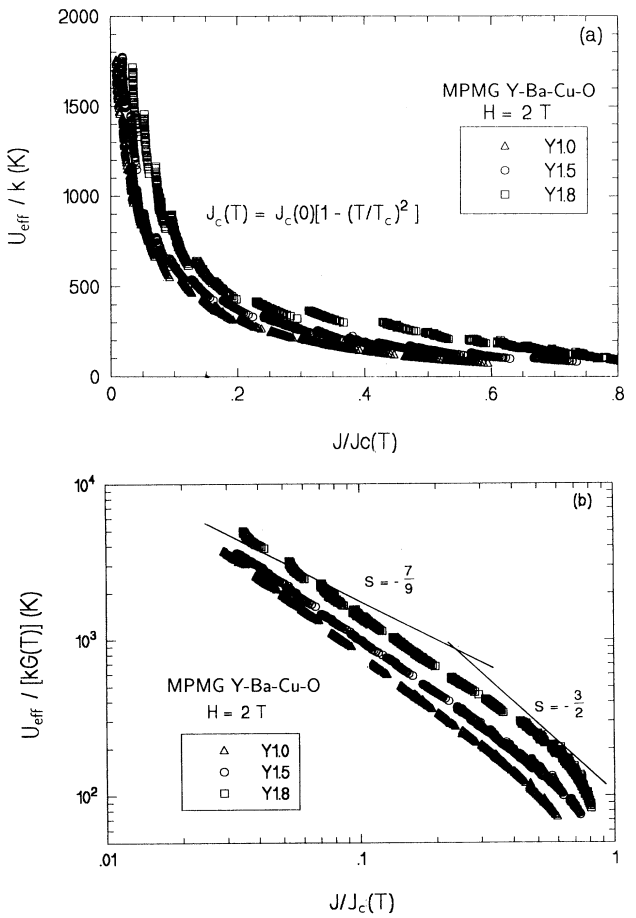


FIG. 13. Plots of (a) $U_{\text{eff}}/k$ versus $J/J_c$ and (b) $U_{\text{eff}}/kG(T)$ versus $J/J_c$ for Y 1.0, Y 1.5, and Y 1.8.

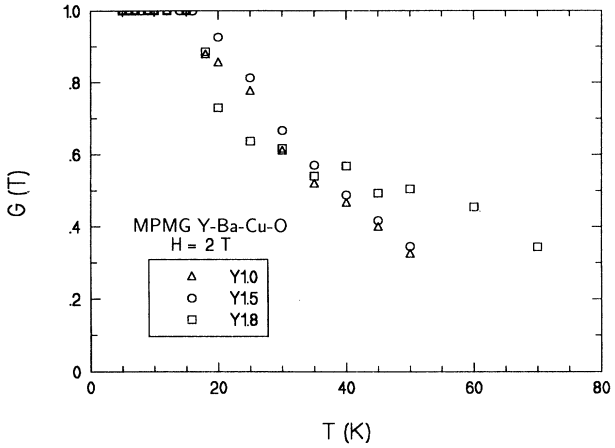


FIG. 14. The numerical data $G(T)$ of the temperature correction to $U_{\text{eff}}(J)$ in Fig. 13.

gime is related to the critical current density $J_c(T)$. This then introduces an additional parametrization of the temperature dependence that effectively shifts the $\ln(dM/dt)$ data along the current-density axis. However, the data now no longer determine unique selections for both $G(T)$ and $J_i(T)$. In order to determine the effect of normalizing current densities, we arbitrarily choose the form $J_c(T)=J_c(0)[1-(T/T_c)^2]$. Notice that, instead of curve-fitting experimental data, this form contains only one value associated with our experiments, i.e., $J_c(0)$, which was obtained from extrapolating $U_{\text{eff}}(J)$ curves as $U_{\text{eff}}$ approaches 0. Figure 13(a) shows the curves of $U_{\text{eff}}$ versus $J/J_c(T)$ for our three samples. Apparently, the high-temperature data points still need a correction along the vertical axis. The aforementioned similar procedure was employed to give Fig. 13(b). The corresponding scaling function $G(T)$ is illustrated in Fig. 14. Comparing these results with those depicted in the last section, we have observed the following.

(i) Less temperature correction is needed for $U_{\text{eff}}$ versus $J/J_c(T)$, which is expected. For the Y 1.8 sample, because of the field- and temperature-driven pinning of low-$T_c$ regions added to the pinning of Y 2:1:1 inclusions, a more anomalous thermal dependence of $U_{\text{eff}}$ is expected. The corrections along the vertical axis are significantly reduced after $J$ is normalized to $J_c(T)$. This can be viewed as a result of the implicit temperature dependence of $J$ on the $U_{\text{eff}}$-$J$ relation.

(ii) It seems that there is no unique way to correct the temperature effect on $U_{\text{eff}}(J)$. However, the assumed $J_c(T)$ scaling does not substantially change the qualitative features of the $U_{\text{eff}}(J)$ functional dependence as shown in Fig. 13(b). Furthermore, $T_x \sim T_{\text{irr}}$ in the $G(T)$ function also suggests that the irreversibility line determines to some extent scaling the $U_{\text{eff}}$ values.

## VII. CONCLUSIONS

Magnetic hysteresis and relaxation measurements have been performed on three MPMG-processed Y-Ba-Cu-O samples with various concentrations of Y 2:1:1 inclusions. The field and temperature dependence of $J_c$ shows that with increasing concentration of Y 2:1:1 inclusions, the enhanced pinning due to the Y 2:1:1 phase is more significant at elevated temperatures and fields. Butterfly-shaped hysteresis loops, which are presumed to be caused by local regions of low-$T_c$ phases, were prominent in the Y 1.8 sample. This behavior leads to an enhanced $J_c$ above $\sim$45 K and influences the effective pinning energy $U_{\text{eff}}$. Using the relaxation data, scaling functions of the effective pinning energy $U_{\text{eff}}$ versus current density $J$, after incorporating the implicit temperature dependence and the field scaling,

$$U_{\text{eff}}(J,T,H)=\frac{U_1}{H^n}G(T)\left[\frac{J_i}{J}\right]^{\mu}$$
$$=\frac{U_1}{H^n}\left[-\left[\frac{T}{T_{\text{irr}}}\right]^2\right]^m\left[\frac{J_i}{J}\right]^{\mu},$$

has been obtained. For $U_{\text{eff}}H^n/kG(T)$ versus $J$ curves, we observed two power-law regimes with $\mu$ equal to $\frac{9}{10}$ and $\frac{3}{2}$ close to the values of $\frac{7}{9}$ and $\frac{3}{2}$, respectively, predicted by the collective flux-creep and vortex-glass models. These power laws are altered somewhat when a temperature dependence for $J_i(T)$ is incorporated. The lack of a universal expression for $G(T)$ in the three MPMG-processed samples is attributed to the presence of pinning centers associated with large concentrations of the Y 2:1:1-phase particles. The samples thus display anomalous field and temperature dependence that is very different from those connected with thermodynamic variables.

The samples with large concentrations of the Y 2:1:1 phase show large enhancements of the entire $U_{\text{eff}}(J)$ curve. Particularly striking is the behavior of the activation energy in the vicinity of the "hump" in the butterfly hysteresis loops, where $U_{\text{eff}}(J)$ at the higher fields crosses above the lower field curves. This is a strong evidence that the "hump" region contributes to a strong field-induced enhancement of the activation energy.

## ACKNOWLEDGMENTS

This work was supported by the United States Department of Energy, Office of Energy Management.

*Permanent address: Department of Materials Science and Engineering, Carnegie Mellon University, Pittsburgh, PA 15213.

[1]D. Dimos, P. Chaudhari, J. Mannhart, and F. K. LeGoues, Phys. Rev. Lett. **61**, 219 (1988).

[2]J. W. Ekin, A. I. Braginski, A. J. Panson, M. A. Janocko, D. W. Capone, II, N. J. Zaluzec, B. Flandermeyer, O. F. de Lima, M. Hong, J. Kwo, and S. H. Liou, J. Appl. Phys. **62**, 4821 (1987).

[3]R. L. Peterson and J. W. Ekin, Phys. Rev. B **37**, 9848 (1988).

[4]M. Suenaga, A. Ghosh, T. Asano, R. L. Sabatini, and A. R. Moodenbaugh, in *High-Temperature Superconductors* (Materials Research Society, Pittsburgh, 1987), Vol. EA-11, p. 247.

[5]M. Tachiki and S. Takahashi, Solid State Commun. **70**, 291 (1989).

[6]T. T. M. Palstra, B. Batlogg, R. B. van Dover, L. F.

Schneemeyer, and J. V. Waszczak, Appl. Phys. Lett. **54**, 763 (1989).
[7]M. Murakami, M. Morita, and N. Koyama, Jpn. J. Appl. Phys. **28**, L1125 (1989).
[8]M. Murakami, Mod. Phys. Lett. **4**, 163 (1990).
[9]M. V. Feigel'man, V. B. Geshkenbein, A. I. Larkin, and V. M. Vinokur, Phys. Rev. Lett. **63**, 2303 (1989).
[10]M. P. A. Fisher, Phys. Rev. Lett. **62**, 1415 (1989).
[11]M. P. Maley, J. O. Willis, H. Lessure, and M. E. McHenry, Phys. Rev. B **42**, 2639 (1990).
[12]M. E. McHenry, S. Simizu, H. Lessure, M. P. Maley, J. Y. Coulter, I. Tanaka, and H. Kojima, Phys. Rev. B **44**, 7614 (1991).
[13]M. Daeumling, J. M. Seuntjens, and D. C. Larbalestier, Nature (London) **346**, 332 (1990).
[14]K. B. Alexander, A. Goyal, D. M. Kroeger, V. Selvamanickam, and K. Salama, Phys. Rev. B **45**, 5622 (1992).
[15]P. McGinn, N. Zhu, W. Chen, S. Sengupta, and T. Li, Physica C **176**, 203 (1991).
[16]S. Jin and J. E. Graebner, Mater. Sci. Eng. B **7**, 243 (1991).
[17]M. Murakami, M. M. Morita, K. Doi, and K. Miyamoto, Jpn. J. Appl. Phys. **28**, 1189 (1989).
[18]A. Goyal, W. C. Oliver, P. D. Funkenbusch, D. M. Kroeger, and S. J. Burns, Physica C **183**, 221 (1991).
[19]Y. Matsui, E. Takayama-Muromachi, and K. Kato, Jpn. J. Appl. Phys. **27**, L350 (1988).
[20]D. J. Werder, C. H. Chen, M. Gurvitch, B. Miller, L. F. Schneemeyer, and J. V. Waszczak, Physica C **160**, 411 (1989).
[21]R. Wang, H. Ren, L. Xiao, Q. He, C. Wang, and D. Yu, Supercond. Sci. Tech. **3**, 344 (1990).
[22]C. H. Chen, J. Kwo, and M. Hong, Appl. Phys. Lett. **52**, 841 (1988).
[23]D. K. Christen and R. Feenstra, Physica C **185-189**, 2225 (1991).
[24]R. Feenstra, D. K. Christen, C. E. Klabunde, and J. D. Budai, Phys. Rev. B **45**, 7555 (1992).
[25]K. Yamaguchi, M. Murakami, H. Fujimoto, S. Gotoh, T. Oyama, Y. Shihara, N. Koshizuka, and S. Tanaka, J. Mater. Res. **6**, 1404 (1991).
[26]K. Yamaguchi, M. Murakami, H. Fujimoto, N. Koshizuka, and S. Tanaka, Physica C **185-189**, 2497 (1991).
[27]M. Murakami, S. Gotoh, H. Fujimoto, K. Yamaguchi, N. Koshizuka, and S. Tanaka, Supercond. Sci. Technol. **4**, S43 (1991).
[28]S. Jin, H. Tiefel, and G. W. Kamlott, Appl. Phys. Lett. **59**, 540 (1991).
[29]P. McGinn, N. Zhu, W. Chen, S. Sengupta, and T. Li, Physica C **176**, 203 (1991).
[30]M. Murakami, H. Fujimoto, S. Gotoh, K. Yamaguchi, N. Koshizuka, and S. Tanaka, Physica C **185-189**, 321 (1991).
[31]M. Murakami, T. Oyama, H. Fujimoto, S. Gotoh, K. Yamaguchi, Y. Shiohara, N. Koshizuaka, and S. Tanaka, IEEE Trans. Magn. **MAG-27**, 1479 (1991).
[32]K. Yamaguchi, M. Murakami, H. Fujimoto, S. Gotoh, N. Koshizuka, and S. Tanaka, Jpn. J. Appl. Phys. **29**, L1428 (1990).
[33]Z. L. Wang, A. Goyal, and D. M. Kroeger, Phys. Rev. B **47**, 5373 (1993).
[34]M. Tachiki and S. Takahashi, Solid State Commun. **72**, 1083 (1989).
[35]T. Izumi, Y. Nakamura, T.-H. Sung, and Y. Shiohara, J. Mater. Res. **7**, 801 (1992).
[36]P. Zhang, L. Zhou, J. Ping, J. Wang, K. Wang, S. Du, and X. Wu, in *Critical Current Limitations in High Temperature Superconductors* (World Scientific, River Edge, 1992), p. 320.
[37]E. M. Gyorgy, R. B. van Dover, L. F. Schneemeyer, A. E. White, H. M. O'Bryan, R. J. Felder, J. V. Waszczak, and W. W. Rhodes, Appl. Phys. Lett. **56**, 2465 (1990).
[38]A. I. Larkin and Y. N. Ovchinnikov, J. Low Temp. Phys. **34**, 409 (1979).
[39]G. M. Stollman, B. Dam, J. H. P. M. Emmen, and J. Pankert, Physica C **161**, 444 (1989).
[40]P. W. Anderson, Phys. Rev. Lett. **9**, 309 (1962).
[41]Y. B. Kim, C. F. Hempstead, and A. R. Strnad, Phys. Rev. Lett. **9**, 306 (1963).
[42]M. R. Beasley, R. Labusch, and W. W. Webb, Phys. Rev. **181**, 682 (1969).
[43]P. J. Kung, M. P. Maley, M. E. McHenry, J. O. Willis, J. Y. Coulter, M. Murakami, and S. Tanaka, Phys. Rev. B **46**, 6427 (1992).
[44]P. J. Kung, M. P. Maley, J. O. Willis, M. E. McHenry, M. Murakami, and S. Tanaka, IEEE Trans. Appl. Supercond. **3**, 1382 (1993).
[45]C. P. Bean, Phys. Rev. Lett. **8**, 250 (1962).
[46]C. P. Bean, Rev. Mod. Phys. **36**, 31 (1964).
[47]A. Umezawa, G. W. Crabtree, J. Z. Liu, W. Weber, W. K. Kwok, L. H. Nunez, T. J. Moran, C. H. Sowers, and H. Claus, Phys. Rev. B **36**, 7151 (1987).
[48]Z. Zeldov, N. M. Amer, G. Koren, A. Gupta, M. W. McElfresh, and R. J. Gambino, Appl. Phys. Lett. **56**, 680 (1990).
[49]M. V. Feigel'man, V. B. Geshkenbein, and V. M. Vinokur, Phys. Rev. B **43**, 6263 (1991).
[50]D. S. Fisher, M. P. A. Fisher, and D. A. Huse, Phys. Rev. B **43**, 130 (1991).
[51]M. V. Feigel'man, V. B. Geshkenbein, and A. I. Larkin, Physica C **167**, 177 (1990).
[52]T. Nattermann, Phys. Rev. Lett. **64**, 2454 (1990).
[53]A. K. Ghosh, M. Suenaga, T. Asano, A. R. Moodenbaugh, and R. L. Sabatini, Adv. Cryog. Eng. **34**, 607 (1987).
[54]M. E. McHenry, M. P. Maley, J. O. Willis, and L. M. Campbell, Phys. Rev. B **40**, 2666 (1989).
[55]P. J. Kung, M. E. McHenry, M. P. Maley, Y. Coulter, and D. E. Peterson, J. Mater. Sci.: Mater. Electron. **3**, 244 (1992).
[56]A. M. Campbell and J. E. Evetts, Adv. Phys. **21**, 199 (1972).
[57]L. F. Schneemeyer, E. M. Giorgy, and J. V. Wasczak, Phys. Rev. B **36**, 8804 (1987).
[58]V. V. Moshchalkov, A. A. Zhukov, D. K. Petrov, V. I. Voronkova, and V. K. Yanovskii, Physica C **165**, 62 (1990).
[59]M. Tinkham, *Introduction to Superconductivity* (McGraw-Hill, New York, 1975).
[60]W. J. Yeh, Z.Q. Yu, S. Labroo, and J. Y. Park, Physica C **194**, 141 (1992).
[61]M. P. Maley, P. J. Kung, J. Y. Coulter, W. L. Carter, G. N. Riley, and M. E. McHenry, Phys. Rev. B **45**, 7566 (1992).
[62]J. G. Ossandon, J. R. Thompson, D. K. Christen, B. C. Sales, Y. Sun, and K. W. Lay, Phys. Rev. B **46**, 3050 (1992).
[63]C. J. van der Beek, G. J. Nieuwenhuys, P. H. Kes, H. G. Schnack, and R. Griessen, Physica C **197**, 320 (1992).
[64]M. E. McHenry, P. J. Kung, M. P. Maley, J. O. Willis, and J. Y. Coulter, IEEE Trans. Appl. Supercond. **3**, 1143 (1993).
[65]J. Mannhart, P. Chaudhari, D. Dimos, C. C. Tsuei, and T. R. McGuire, Phys. Rev. Lett. **61**, 2476 (1988).
[66]T. Matsushita, S. Funaba, Y. Nagamatsu, B. Ni, K. Funaki, and K. Yamafuji, Jpn. J. Appl. Phys. **28**, L1508 (1989).
[67]T. Matsushita and B. Ni, IEEE Trans. Magn. **TM-25**, 2285 (1989).